THE UNIVERSITY OF CALGARY

Measurement of Neutron Contamination in 15 MV and 18 MV X-ray Beams

by

Muriel Patricia Loye

A THESIS

SUBMITTED TO THE FACULTY OF GRADUATE STUDIES

IN PARTIAL FULFILMENT OF THE REQUIREMENTS FOR THE

DEGREE OF MASTER OF SCIENCE

DEPARTMENT OF PHYSICS AND ASTRONOMY

CALGARY, ALBERTA

AUGUST, 1997

Abstract

High energy radiotherapy x-ray beams (> 10 MV) are unavoidably contaminated by neutrons. This study intercompares the response of 3 neutron detectors and estimates the neutron dose equivalence in 15 and 18 MV x-ray beams. The neutron detectors used were: 1) Phosphorous Pentoxide powder, 2) a moderated Indium foil, and 3) a Superheated Drop Detector (SDD). The recently marketed SDD was assessed to determine its suitability for neutron dose equivalence measurements. The P_2O_5 results were considered the standard and they demonstrated that neutrons contribute < 0.40% and < 0.07% of the total dose administered by the 18 and 15 MV beams, respectively. The Indium foil used a conversion factor calculated by Rogers and Van Dyk [1981] resulting in computed neutron doses 1000 times larger than the P_2O_5 results. It is not known why. Compared to the P_2O_5 results the SDD underestimated the neutron dose equivalence by a factor of two.

Acknowledgments

I would like to acknowledge the help and support of the staff at the Tom Baker Cancer Centre. I also very much appreciated their encouragement and many smiles. I am especially indebted to John Kollar for his patience, and his help with my computer problems.

I am grateful to Gavin Stuart, Director, Tom Baker Cancer Centre, for his gift of financial summer support.

I would like to especially thank my supervisor, Dr. N. Sidhu, for providing me the opportunity to explore the field of medical physics.

Table of Contents

List of Tables

List of Figures

Chapter 1

Introduction

Several treatment protocols and modalities are commonly available to a patient diagnosed with cancer. Surgery, chemotherapy, radiotherapy, or a combination of these are conventional techniques available to the oncologist for treatment prescriptions with curative or palliative intent. Radiotherapy prescriptions vary depending on the site, type, and staging of the tumour. The radiation dose, beam type, beam energies, treatment geometry, and target volume are some of the parameters that must be prescribed and planned for treatment. High energy x-rays and electrons are the conventional types of radiation beams utilized. The tolerance of normal tissue defines the radiation dose limits thus in order to allow normal tissue to repair itself the radiation dose is fractionated. The total radiation dose prescribed to the target volume is the number of fractions multiplied by the daily dose. The goal of radiation therapy is to administer a lethal total dose to a target volume while minimizing the dose to the surrounding healthy tissue.

Patients are usually treated on medical electron linear accelerators (LINACs) which generate x-ray and electron beams at megavoltage energy. Via thermionic emission, electrons are boiled off a cathode in the accelerator's electron gun and undergo an initial acceleration while crossing the potential difference created by the presence of an anode. A pulsed modulator gives high voltage pulses to both the electron gun and a Klystron (or magnetron) radiofrequency (RF) power source. In standing wave accelerators the Klystron gives off a microsecond pulse of electromagnetic radiation to the

accelerator guide which is reflected back and forth within the accelerator cavities to create the standing wave. The high energy electron beam created may be converted to a bremsstrahlung x-ray beam using a high atomic number target.

Figure 1.1 depicts the treatment head of a medical LINAC. The target and collimators generate and define the useful x-ray radiation beam respectively. A flattening filter modifies the highly forward peaked bremsstrahlung intensity distribution to produce a more uniform (flat) intensity profile across the beam.

X-ray beams of energy 10 MeV or greater produce neutrons in a (γ,n) reaction with beam line elements. Neutrons are produced in the target, collimator jaws, lead shielding, the air path of the beam, and in the patient [Nath *et al.*, 1986]. For many years it was recognized that these 'contaminant' neutrons were potentially

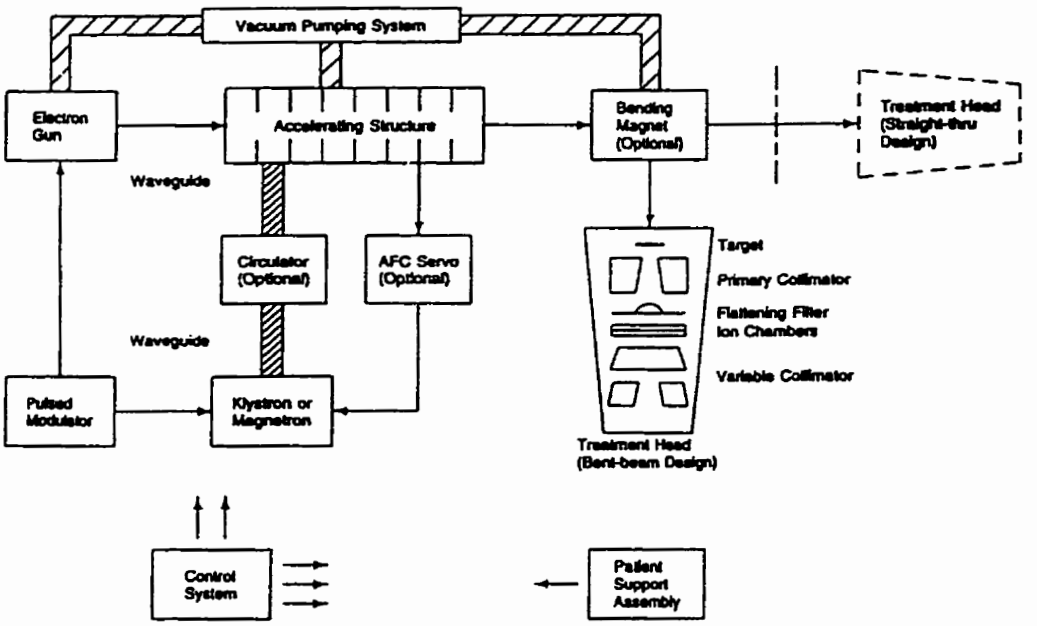

Figure 1.1 LINAC schematic

hazardous to the patient [Ing *et al.*, 1982; Nath *et al.*, 1984; Swanson, 1980] but the

neutron flux generated was unknown and dependent upon the accelerator design. McCall *et al.*, [1984] and Nath *et al.*, [1986] showed that the neutron fluence within the treatment beam is limited to less than 0.04% of the given photon fluence for various machines and can be deemed an insignificant addition to the dose received by the patient. Price *et al.*, [1978] using phosphorous pentoxide detectors in a 25 MV x-ray beam of a Sagittaire machine found the ratio of neutron dose to photon absorbed dose within the beam to be between 0.2 and 0.5 percent. Outside the beam they found the ratio to be 0.12 percent.

Ing and Shore [1982] and Stranden [1976] concluded that the neutron dose due to induced activity within patients is very low. Their results indicated that the dose delivered outside the primary beam by scattered photons is approximately 1500 times that of the dose delivered by neutrons produced in tissue by photonuclear reactions for beam energies above the (γ,n) reaction threshold. Hence, neutron production within tissue is not very important as a source of unwanted irradiation.

Neutron detector development has been ongoing for several decades. Nath *et al.*, [1986] and McCall *et al.*, [1984] have investigated their use for measuring neutron dose surrounding linacs. Measurements within the treatment room have been concerned with the detection of neutrons within the primary beam and those scattered through the treatment room. Moderated thermal neutron detectors and fast neutron activation detectors have been used inside and outside the x-ray beam [Nath *et al.*, 1986; Rogers and Dyk, 1981]. Scintillation detectors and ionization chambers have been used by various researchers for the purpose of detecting scattered, thermalized neutrons outside of the primary beam but still inside the treatment room [Rogers, 1979; Nath *et al.*, 1979; McCall

et al., 1984; Stranden, 1976].

For the LINACs used in this study neutrons are produced mainly by x-ray interactions. At the beam energies produced by medical linacs neutron production through electrodisintegration (electron interaction) is approximately two orders of magnitude smaller than neutron production through photodisintegration (gamma or x-ray interaction) [McGinley *et al.*, 1976; McCall *et al.*, 1984]. Further discussion on the theory of neutron production can be found in section 1.1. Due to the pulsed nature of the photon beams produced by the medical linear accelerators detection of neutrons is a difficult task. One difficulty lies in finding a suitable neutron detector that will not be influenced or oversaturated by the high intensity x-rays of the primary beam. Even after transmission through the treatment head shielding the photon leakage flux outside the primary beam is 10-100 times greater than the neutron flux [Nath *et al.*, 1986]. In the unattenuated primary beam the photon flux is 1000-4000 times greater than the neutron flux. These numbers indicate a need to use passive neutron detectors within the treatment room.

Passive detectors are those that do not depend on electronics to enable the desired interactions to be counted and thus will not be influenced by the photon flux. An example of a passive detector is an activation detector where the neutrons induce radioactivity in the detector material. The radioactivity may then be counted by another radiation detector outside of the influence of the x-ray flux.

To be able to predict the neutron dose acquired the energy of the neutron must be known, thus, another inherent problem with neutron detection is the dependence of dose equivalence on the neutron energy spectrum because a neutron's quality factor (and thus

the dose equivalence) depends on its energy [Bading *et al.*, 1982]. This produces a need to estimate a neutron energy spectrum by using a neutron fission spectrum from a source like Californium-252, or by means of a computer calculated spectrum, or by experimental procedure using a spectrometer (like a Bonner Sphere Spectrometer). These solutions also have difficulties which will be discussed in the following chapters.

In this thesis the use and comparison of three different neutron activation detectors is presented. The neutron dose was determined for 15 and 18 MV x-ray beams from a Varian Linac using three detectors and their results were compared. The first detector studied was the phosphorous pentoxide P_2O_5 powder. This neutron detector has a well documented history of use [Price *et al.*, 1978; Nath, 1980; Bading *et al.*, 1982] and has been proven reliable for the detection of both fast and thermal neutrons. The second detector, an Indium foil, has also been the subject of several investigations [Stephens and Smith, 1958; McCall *et al.*, 1979; Rogers and Dyk, 1981]. This foil is a thermal neutron detector so a moderator must be used in conjunction with the detector to measure fast neutron flux. The third detector, a Superheated Drop Detector (SDD), has a relatively recent history compared to the other detectors used. It is called a Neutrometer-HD™ and is claimed by the manufacturers to be reliable and simple to use [Apfel and Roy, 1984; Nath *et al.*, 1993].

1.1 Theory

When electromagnetic radiation or charged particles enter a material, electromagnetic interactions may take place. Ionization is the removal of an electron from an atom resulting in an ion which is an atom with a net positive charge. This occurs when an electron absorbs sufficient energy to break away from its orbital shell within the parent atom. Electrons and charged particles are directly ionizing, whereas neutrons and photons (both of which are electrically neutral) are indirectly ionizing. This implies that neutrons and photons need an atomic or nuclear interaction, which results in a full or partial transfer of energy, to produce a secondary emission of a charged particle so ionization can occur.

1.1.1 Definitions

Absorbed Dose, D, is the mean energy (ε) imparted by ionizing radiation per unit mass (m) of the irradiated material as shown by the equation,

$$D = \frac{d\bar{\varepsilon}}{dm} \tag{1.1}$$

given by the International Commission of Radiation Units [ICRU #33, 1980]. The units of absorbed dose are in joules per kilogram (J/kg) also referred to as a Gray.

Linear Energy Transfer (LET) for a charged particle beam is defined as,

$$L = \frac{dE}{dl}\Big|_{\Delta} \qquad (1.2)$$

where dE is the average energy less than Δ locally imparted to a medium by a charged particle of specified energy in travelling a distance dl [ICRU #33, 1980]. It is expressed in keV/μm.

There is a wide variation in the way energy is transferred depending on the energy and type of radiation. If dealing with monoenergetic radiation then the particles' path lengths would be similar and LET would be meaningful. However most radiations consist of a wide spectrum of energies. This implies that LET can only be an average of the energies per track length. An average is not useful if the variation is great between the quotients (or LETs). There are two ways to calculate LET. First, the track or path is divided into equal energy increments, giving the energy average. Second, the track average can be found by finding the energy per equal track/path increment. These averages can differ substantially for the same radiation [Hall, 1988].

Radiobiological Effectiveness (RBE) is a measure of how a test radiation compares to a standard radiation, as defined by,

$$RBE = \frac{D_{250}}{D_r} \qquad (1.3)$$

Here D_{250} refers to the given dose of 250 kV x-rays, and D_r refers to the given dose of the test radiation so that both doses have the same biological effect or endpoint.

All ionizing radiations are able to produce the same kind of biological effect.

However, if the radiation types are not the same equal absorbed doses of the radiations may not give rise to the same biological effects. To be able to intercompare radiations based on their biological effect dose equivalence has been defined for the low doses of radiation normally encountered in the field of radiation protection not for assessing the effects of high-level, accidental exposures to radiation [ICRU #33, 1980].

Dose Equivalence is obtained by weighting the absorbed dose with certain modifying factors depending on the type of radiation and the conditions of irradiation [ICRP #15, 1969]. One factor is the quality factor (Q), which weights the absorbed dose depending on the predetermined biological effectiveness of the radiation type. The factor Q is closely related to RBE but unlike RBE it does not consider the organ, tissue or biological endpoint [ICRU #33, 1980]. Dose equivalence is defined by the ICRU #33 as the product of the absorbed dose, D, and the quality factor, Q, that characterizes that particular radiation,

$$\mathbf{H = DQN} \qquad (1.4)$$

where N is the product of all other modifying factors recommended for weighting the absorbed dose by the ICRP (International Commission of Radiation Protection). N is currently assigned the value of 1 for external source irradiations [ICRU #33, 1980]. The units for dose equivalence are also in joules per kilogram, but is also referred to as a Sievert (Sv).

The value of neutron dose equivalence at the treatment site can rarely be determined directly. One way is to use a 'Rem-meter' which comprises of a spherical

moderator placed around a thermal neutron activation detector (rem-meters will be discussed in detail in Chapter 3). Otherwise the neutron dose equivalence must usually be derived from measurements of neutron fluence incident upon the body and use of conversion (fluence to dose equivalence) factors specified by the International Commission on Radiation Protection [ICRP #51, 1987], or experimentally determined conversion factors. The calculations for determining dose equivalence will be explained in greater detail in chapters 2 and 3.

1.1.2 Neutron Production

Electrons and x-rays usually initiate the reactions that produce the neutrons we are studying. This is due to the way x-rays are created in LINACs. Electrons at high energies are directed towards a target manufactured from a high atomic number material. The majority of the x-rays are produced by the deceleration of electrons within this target. The radiative energy losses, or bremsstrahlung losses, by the electrons are proportional to the stopping power of the material of the target and are therefore proportional to Z^2 (where Z is the atomic number of the target material). This is why a high atomic number material like tungsten is used as a component for the target of a LINAC.

Neutron production can occur within any area of the LINAC in which electrons or photons are interacting with matter. They can also be produced in the path that the x-ray beam takes from the target to the patient. Neutrons can be removed from their parent nucleus with a minimum input of energy of 6-16 MeV for most stable nuclei with an atomic number greater than that of carbon (Z = 6) [McCall *et al.*, 1984]. The incident

particle that gives the energy to the target nuclei will be either a photon or an electron. These reactions that remove the neutron are called photodisintegration and electrodisintegration respectively.

Figure 1.2, a schematic of photodisintegration, depicts an incident electron of energy E_i being decelerated by a radiator target nucleus R and hence, producing a bremsstrahlung x-ray. A second interaction may occur in or around the target, up to several meters away. If the energy of the incident photon is high enough a neutron can be removed from the nucleus A.

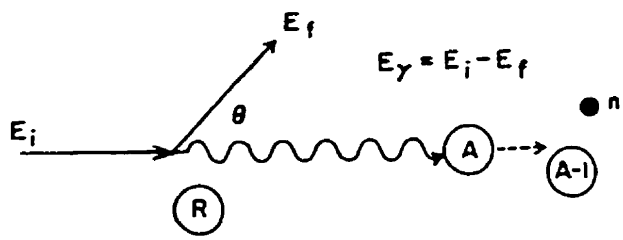

Fig. 1.2 Photodisintegration (γ, n) [McCall *et al.*, 1984]

Figure 1.3 demonstrates electrodisintegration. Here the radiator nucleus and the nucleus that has the neutron removed are one and the same. The energy needed by the nucleus to release a neutron is transferred from the electron by means of a 'virtual' photon. The electron is deflected from its original path as in the first case but no actual photon is detected. Therefore the virtual photon is used to explain the energy transfer. The

electrodisintegration reaction can be considered as (e,n) or (e, e'n). It depends only on whether the electron with the final energy can be detected.

A neutron is not always the result of photons or electrons interacting with matter, otherwise we would be overwhelmed with neutrons. There are many possible results of these nuclear interactions. The *cross-section* of a reaction is a means of describing the

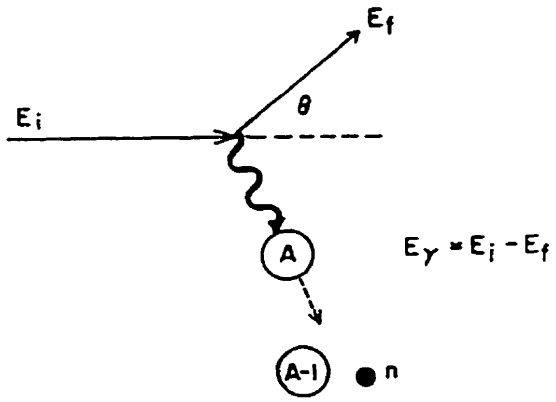

Fig. 1.3 Electrodisintegration (e, n) [McCall et al., 1984]

probability of an interaction occurring, and is given in the units of barns/atom or cm^2/atom [Krane, 1988].

Knowledge of cross-sections indicates that with increasing incident particle energy there will be an increasing probability of neutron production occurring up until a certain maximum energy, after which it decreases. This curve is called the 'giant resonance' due to the reaction behaving like a resonance reaction [McCall *et al.*, 1984]. Resonance means the reaction may proceed only if the photon (or electron) has exactly the resonance energy. McCall *et al.*, [1984] state that in theories of photonuclear reactions this

resonance is attributed to the electric dipole absorption of the incident photon. The area under this curve is sometimes called the 'strength' of the giant resonance and is given by an approximation of the dipole sum rule [Bethe, 1954; Jackson, 1975].

The cross-sections for a (γ,n) and (e,n) reaction, indicate that photodisintegration, rather than electrodisintegration, is the predominant interaction mechanism for producing neutrons in medical LINACs [Swanson, 1978]. This is due to the fact that the elements composing the patient (H, C, N, O), and in treatment head materials (Pb, W, Cu, etc), have their giant resonance for photodisintegration reaction at lower energies than the giant resonance for electrodisintegration reaction.

1.1.3 Interaction of Neutrons and Matter

Neutrons have no electrical charge. Therefore they do not interact in matter by means of the Coulomb force, which dominates the energy loss mechanisms for charged particles [Krane, 1988]. Neutrons have a large mean free path compared to their charged particle counterparts, and negligible interactions occur with atomic electrons. A neutron, even one with low energy, can penetrate the nucleus, experience the nuclear force, and start nuclear reactions. A result of this reaction will be the emittance of secondary radiation. The specific type of secondary radiation will depend on the incident neutron energy, the type of target nuclei and the cross section for the particular reaction. For high energy or fast neutrons, described in this project to be a neutron above thermal energies (> 0.025 eV), reactions such as (n,p), (n,α), or (n,2n) and scattering are possible. The slow or thermal neutrons' main interaction, besides scattering, is radiative capture (n,γ)

[Krane, 1988].

A scattering interaction between the nucleus and neutron means the neutron's path is changed or deflected either elastically (with energy conserved between interacting particles), or inelastically (with energy not being conserved between interacting particles but being lost in the form of gamma rays). Slow neutrons, generally considered to be less than 0.5 eV have a high probability for elastic collisions which bring these slow neutrons into thermal equilibrium with the absorber material. Being 'thermal' neutrons, radiative capture (n,γ) is usually the most probable interaction [Krane, 1988]. A fast neutron will be slowed, or 'moderated', by the scattering processes in the absorbing material until it loses enough energy to be radiatively captured by a nucleus of the absorbing material. Otherwise the fast neutron will interact directly with a nucleus to produce a secondary emission, like one of the previously described reactions. This scattering interaction is most effective for moderating a neutron's energy when the scattering material consists mainly of hydrogen. Neutrons can most efficiently transfer their energy in the form of kinetic energy through elastic collisions when the target nucleus is of approximately the same mass.

All neutron interactions (except elastic collisions) produce secondary emissions such as, gamma rays, fast recoil protons, and alpha particles. The absorbed dose from the neutrons is technically due to these secondary charged particles, rather than the neutron itself; this is called indirect ionization. Most of the particles set in motion by neutrons are massive compared with electrons, which are excited and ionized from their atomic nuclei by gamma and x-rays. The difference in mass between electrons and the heavier

secondary emissions (such as protons) accounts for the differences in the biological effects observed between equal absorbed doses of x-rays and neutrons [Hall, 1988].

Chapter 2

Experiment 1 - Phosphorous Pentoxide

The phosphorous pentoxide (P_2O_5) powder neutron detector has been well documented and found to give accurate results to within about 4 percent for a fast neutron flux and to within about 13 percent for a thermal flux [Price *et al*, 1978]. Bading *et al.*, [1982] found they could measure neutron surface dose rate with uncertainties of approximately 25 percent. Radioactivity is induced in the phosphorous of P_2O_5 powder and it is able to detect both fast and thermal neutrons. Different nuclear reactions take place in the phosphorous depending on the energy of the neutrons involved in the interactions. The reactions induced in the powder are numerous when irradiating this activation detector with neutrons and high energy x-rays. Most of the reactions produce either stable daughters or daughters with a short half life. Table 2.1 shows the various reactions expected for this experiment and the emitted radiation. These will not interfere with counting of the two reactions whose daughter products have a suitably long half life and characterize the interactions of interest. These are the (n,p) reaction for fast neutrons and the (n,γ) radiative capture reaction produced by thermal neutrons. The $^{31}P(n,p)^{31}Si$ reaction has a product half-life of 2.62 hours and the Silicon-31 decays by emission of beta particles of energy 1.48 MeV. This reaction has a threshold neutron energy of 0.7 MeV, meaning that some intermediate fast neutrons will not react with a phosphorous atom. Photonuclear processes in the oxygen and phosphorous produce neutrons which in turn

activates the ^{31}P and leads to ^{31}Si activity. Price et al, [1978] did

Table 2.1 P_2O_5 nuclear reactions when irradiated [Price *et al.*, 1978].

Reaction	Product Half Life	Radiation	% Emission
$^{31}P(n,\gamma)^{32}P$	14.28 d	1.71 β^-	100%
$^{31}P(n,2n)^{30}P$	2.5 min	3.24 β^-	99%
$^{31}P(\gamma,n)^{30}P$		0.511 γ	200%
		2.230 γ	0.5%
$^{31}P(n,p)^{31}Si$	2.62 h	1.48 β^-	99%
		1.26 γ	0.07%
$^{31}P(n,\alpha)^{28}Al$	2.31 min	2.85 β^-	100%
		1.78 γ	100%
$^{31}P(n,np)^{30}Si$	Stable		
$^{31}P(\gamma,2n)^{29}P$	4.45 sec	3.95 β^-	99%
		0.511 γ	200%
		1.28 γ	0.8%
		2.43 γ	0.2%
$^{31}P(\gamma,p)^{30}Si$	Stable		
$^{31}P(\gamma,np)^{29}Si$	Stable		
$^{16}O(n,\gamma)^{17}O$	Stable		
$^{16}O(n,2n)^{15}O$	123 sec	1.74 β^+	100%
		0.511 γ	
$^{16}O(n,p)^{16}N$	7.14 sec	10.4 β^-	26%
		4.27 β	
		2.75 γ	1%
		6.13 γ	69%
		7.11 γ	5%
$^{16}O(n,\alpha)^{13}C$	Stable		
$^{16}O(n,np)^{15}N$	Stable		
$^{16}O(\gamma,2n)^{14}O$	70.91 sec	4.12 β^+	0.6%
		1.811 β^+	99%
		0.511 γ	200%
		2.312 γ	99%
$^{16}O(\gamma,n)^{15}N$	Stable		
$^{16}O(\gamma,np)^{14}N$	Stable		

a study of these interactions to discover the extent of the interference. It was determined

that the photonuclear interference, where the photon flux is approximately 1300 times larger than the neutron flux, is roughly 3%.

The $^{31}P(n,\gamma)^{32}P$ thermal reaction has a product half-life of 14.28 days and also emits a beta particle with an energy of 1.71 MeV. This allows the determination of the ^{31}Si activity induced by fast neutrons and ^{32}P activity induced by thermal neutrons after irradiation by counting the sample at different times (approximately 24 hours later). Since both products are beta emitters a liquid scintillation counter (LSC) can be used to measure the induced activity. These reactions can distinguish between the fast and thermal neutrons. However to convert the total flux to dose equivalence a knowledge about the complete neutron energy spectrum is required.

The cross-section for the $^{31}P(n,\gamma)^{32}P$ reaction to detect thermal neutrons is 0.190 barns [Garber and Kinsey, 1976], whereas the cross-section for the $^{31}P(n,p)^{31}Si$ reaction to detect fast neutrons is dependent upon the energy of the neutrons (see figure 2.1) [Price *et al*, 1978]. One can see that the threshold neutron energy for detection of fast neutrons is 0.7 MeV and the probability of the interaction increases with increasing neutron energy. When the neutron energy reaches approximately 3 MeV, the cross-section stays roughly constant around 0.1 barn with increasing energy.

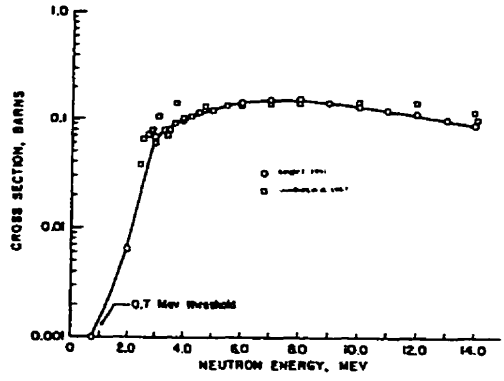

Fig. 2.1 $^{31}P(n,p)^{31}Si$ cross section verses neutron energy [Price *et al.*, 1978]

2.1 Methods and Materials

The phosphorous pentoxide powder deliquiesences quickly when in contact with any moisture including that in air. Due to this high reactivity with water, precautions, such as using a fume hood, had to be taken when preparing samples. Because the powder for this activation material is so difficult to handle, a solution was developed using distilled water which enabled the irradiations to proceed smoothly. The best mixture was found to be 0.32 grams of powder per milliliter of distilled water. Five milliliters of this solution were placed in scintillation vials for irradiation. The samples were irradiated with 4000 MU (monitor units) of x-rays delivering approximately 40 Gray of dose (depending on the field size). Following irradiation 2 ml of the solution was added to the LSC cocktail Insta-gel™ to be counted. Price et al, [1978] in their experiments irradiated the powder and then proceeded to create a solution with distilled water to which they added their LSC cocktail. The method used in this project was also used by Bading et al, [1982]. They

added 3 ml of the solution to the LSC cocktail instead of the 2 ml added in the present work. Through experimentation with various amounts of solution, it was determined that 2 ml of solution (rather than the 3 ml used by Bading et al., [1982]) added to the LSC cocktail gives a much clearer solution which is highly desired for liquid scintillation counting. 3 ml of solution added to the cocktail produced a cloudy gel which the LSC found to be uncountable.

One of the variables of the experiment were the primary photon beam energy spectra of 15 and 18 MV, to determine the amount of neutrons produced for these two spectra. The field sizes of the beam were changed from 5x5 cm^2 up to 40x40 cm^2 to determine if the neutron production varied with field size. As well the location of the vials were placed so as to produce a neutron dose equivalent profile for each of the field sizes used. This was done to ascertain whether or not the neutron profiles varied in any way from the photon profile for the same beam size. The vials, filled with the phosphorous detector solution, were placed in locations starting from the isocenter of the beam to 30 cm outside of the beam edge along the inplane axis on the patient plane (perpendicular to the beam).

The dose was administered with a dose rate of 600 monitor units per minute, where one monitor unit equals approximately one centi-Gray (cGy), depending on the field size of the trial in question. The LINAC units are calibrated so that one monitor unit (MU) of given photon energy equals one centi-Gray of photon dose for a 10x10 cm^2 field size at a reference depth in water. For differing field sizes a collimator scatter correction factor is used to change the exact relationship between monitor units and centiGray of

radiation.

Immediately after irradiation two milliliters from each sample were placed in fresh scintillation vials so that any residual radioactivity occurring within the vials would not interfere with the counting activity from the irradiated powder and distilled water solution. These vials were then refrigerated for 5 to 10 minutes because it was found that mixture with the liquid scintillation cocktail produced less visible (colour) quenching if both substances were cool. The scintillation process entails the conversion of part or all of the kinetic energy of the beta particles to light photons as the particle is slowed and/or stopped in the scintillation detector material. This light or fluorescence is created by an atom in certain materials from the absorption of the kinetic energy of a charged particle passing nearby. Fluorescence is the prompt emission of visible radiation from a substance following its excitation. The scintillation material is an organic solvent (like toluene) with small amounts of organic compounds (solutes) and is called a liquid scintillation cocktail. This project used Insta-gel Plus™ as the cocktail which was a blend of pseudocumene (1,2,4 trimethylbenzene) 80-90% with scintillators PPO and BIS - MSB emulsifiers. The photon emitted has less energy than the minimum needed for absorption. Thus there is very little overlap between the optical absorption and emission spectra, implying there is little self absorption of the fluorescence. Another benefit of using liquid scintillation counting is the fact that the sample is totally immersed in a scintillation material and enables a counting efficiency of close to 100%.

The light photons produced are then detected by the photocathodes of two photomultiplier tubes. These photocathodes emit electrons when they are struck by a

photon. Through an increasing voltage potential the electrons are attracted to a series of dynodes where a multiple of electrons are given off at each dynode. Whenever output pulses from each of the two photomultiplier tube occur within 25 nanoseconds of each other then they are considered to be coincident and thus true rather than random events. Using a coincidence counting technique reduces the noise.

In each vial, 15 milliliters of Insta-gel Plus™ scintillation cocktail was used. Eight to ten vials were irradiated and counted in a trial at any one time, these included two vials for background counts. The vials were counted for one minute each, eight to ten times. These counts were corrected for decay time, then averaged and used in the calculations and data analysis. The counts determining the ^{32}P activity for the thermal neutrons were detected the next day after sufficient decay time of approximately 20 to 24 hours had elapsed so that no significant counts from ^{31}Si would be detected. The same vials were again placed in the LSC and each vial was counted for 10 minutes approximately 5 times.

2.2 Data Analysis

Using the results from the experiments, the neutron dose equivalence can be found. This was accomplished by first using the statistically significant count rate to determine the saturation activity of the sample. The next step was to calculate the total flux of neutrons using an estimated neutron spectrum (for the fast neutron flux) and the cross-section for $^{31}P(n,p)^{31}Si$ reaction. The dose equivalence was computed by using ICRP fluence to dose equivalent conversion factors.

First it must be decided whether the counts collected from the liquid scintillation counter (LSC) are statistically significant or not. We defined "statistically significant" to be greater than the background counts by three times the standard deviation (σ). Differences greater than 3σ were considered significant since there is a less than 1% chance that the counts are due to random error [Sorenson and Phelps, 1987].

The measured activity (A_t), in disintegrations per second, of the phosphorus sample was computed using the equation, [Price *et al.*, 1978],

$$A_t = \frac{C_t m}{0.64\varepsilon} \tag{2.1}$$

where C_t is the counts per second found in a 2 ml (or 0.64 g) portion of the irradiated sample, and now has units of counts/second/gram. m is the mass of the total irradiated 5 ml sample. ε is the counting efficiency and was determined to be 95% for ^{31}Si and ^{32}P [Price *et al*, 1978].

Once the measured activity of each sample was found then the saturation activity could be calculated. Towards this end the number of target atoms available in each 5 ml sample needed to be found. This was accomplished using the equation,

$$N_{plus} = (N_A mna) \cdot A \tag{2.2}$$

where N_A is avogadro's number, m is the mass of the sample (1.6 grams), n is the number of target atoms per molecule, a is the natural occurrence of phosphorus (^{31}P) which is

1.00, and A is the molecular weight. It was found that N_{phos} was 1.36×10^{22} atoms.

The saturation activity (A_s), in disintegrations per second of phosphorous, is the maximum achievable activity per target atom of the irradiated sample. It may be determined using the acquired count rate, assuming irradiation proceeded for a time t_o, at which time the sample was removed from the radiation with an activity A_o.

$$A_o = A_s(1 - e^{-\lambda t_o}) \tag{2.3}$$

Figure 2.2 depicts how the activity of a sample changes with time as it is being irradiated until time t_o, and how the activity continuously decays.

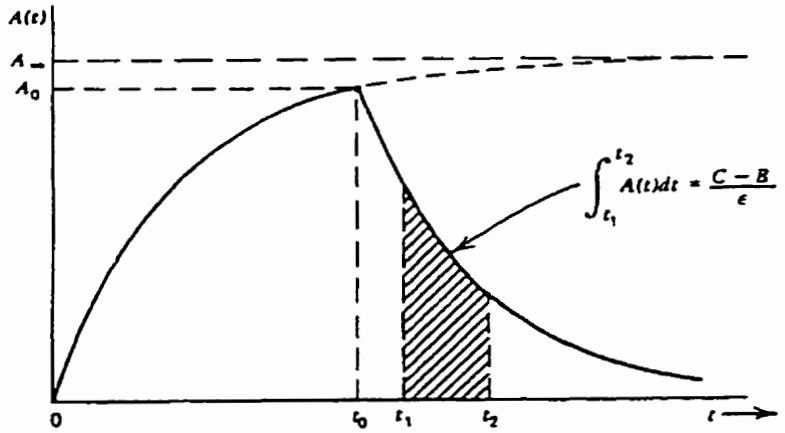

Figure 2.2 Graphical representation of the induced activity of a sample [Knoll, 1989].

Due to this continuous decay, all times involved must be carefully accounted for. If the counting of the activity is carried out over a time period between t_1 and t_2 then the number of counts found will be,

$$C = \varepsilon \int_{t_1}^{t_2} A_o e^{-\lambda t} dt + B = \varepsilon \frac{A_o}{\lambda}(e^{-\lambda t_1} - e^{-\lambda t_2}) + B \qquad (2.4)$$

where B is the background counts found during the time of counting and λ is the decay constant of the product in question. By combining equations 2.4 and 2.3 one can find,

$$A_s = \frac{\lambda (C - B)}{\varepsilon (1 - e^{-\lambda t_a})(e^{-\lambda t_1} - e^{-\lambda t_2})} \qquad (2.5)$$

From equation 2.5 it can be rearranged as Price *et al* [1978], has done,

$$A_s = \frac{A_t(\lambda t_c) \exp(\lambda t_w)}{N_{phos} [1 - \exp(-\lambda t_i)] [1 - \exp(-\lambda t_c)]} \qquad (2.6)$$

N_{phos} is the number of target atoms of ^{31}P in the irradiated sample, and t_c , t_w , and t_i are the times for counting, waiting (time elapsed between irradiation and counting), and irradiation respectively. A_t is the measured activity of the sample and was determined using equation 2.1.

Once the saturation activity of ^{31}Si for each sample is calculated then the total flux of the fast neutrons can be determined in n/cm^2-s using the equation,

$$\Phi_F = \frac{A_s(^{31}Si) \int_{E_{th}}^{E_{max}} \phi_n(E)dE}{\int_{E_{th}}^{E_{max}} \phi_n(E)\ \sigma_{n,p}(E)dE} \qquad (2.7)$$

From the saturation activity of ^{32}P the total flux of thermal neutrons can be determined in n/cm^2-s, using the following equation,

$$\Phi_{th} \qquad \frac{A_S(^{32}P)}{\sigma_{n,\gamma}} \qquad (2.8)$$

where σ denotes the cross-section of the reaction of interest (either n,γ or n,p) and, $\phi_n(E)$ is the differential neutron energy spectrum used. Since the differential neutron energy $\phi_n(E)$ appears in the denominator and numerator of equation 2.7, a relative neutron energy spectrum is sufficient rather than an absolute neutron energy spectrum. The TLD/BSS and Cf-252 spectra were normalized at 0.7 MeV energy level where P_2O_5 has its detection threshold.

In order to obtain the fast neutron flux an estimation of the neutron spectrum must be made. Two neutron spectra were investigated in this project to discover which would be a better estimation of the neutron spectrum surrounding a 15 or 18 MV LINAC. In the primary beam, the average neutron energy at a point in the primary photon beam does not change greatly with increasing peak photon energy [Nath *et al*, 1986]. Thus it was assumed that the same spectrum may be used for both primary photon energies (15 and 18 MV). One of the spectra used was the neutron fission spectrum for Californium-252, (see figure 2.3) [Batenkov, 1983].

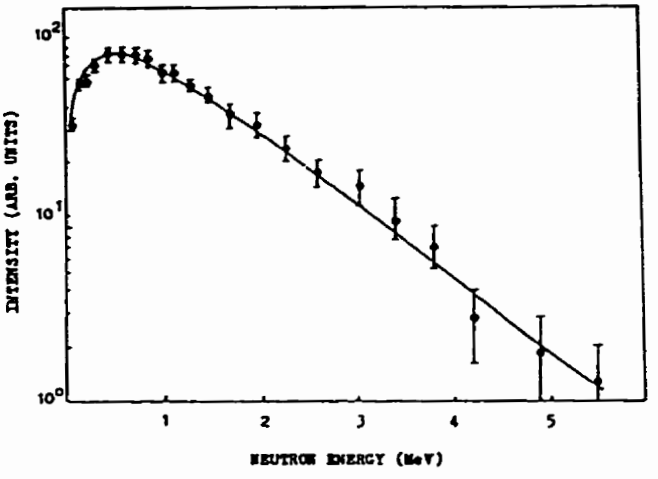

Fig. 2.3 Differential neutron energy spectrum for Cf-252.

The neutron spectrum of a LINAC has been found to be degraded compared with a fission spectrum outside of the field due to moderation by the shielding and the collimators [Nath *et al*, 1986]. Even with the degradation of the spectrum outside of the treatment field the californium-252 fission spectrum should be a good approximation of the expected neutron spectrum because it has an average neutron energy of approximately 1 MeV, close to the recommended values of 2.0 MeV for 18 MV and 1.8 MeV for 15 MV spectra [Nath *et al.*, 1986].

The second neutron spectrum used was determined experimentally by Dr. James Liu [unpublished, 1995] using Thermoluminescent Dosimeters within a Bonner Sphere Spectrometer (TLD/BSS) for a 15 MV LINAC (see figure 2.4). The position of detection was 1 meter above the x-ray target with the accelerator gantry at the zero position. The results will give us a good approximation of the spectrum after it has been degraded by the shielding but there might be error involved for the detectors placed within the open beam.

In other words this spectrum might underestimate the neutron energies within the primary beam.

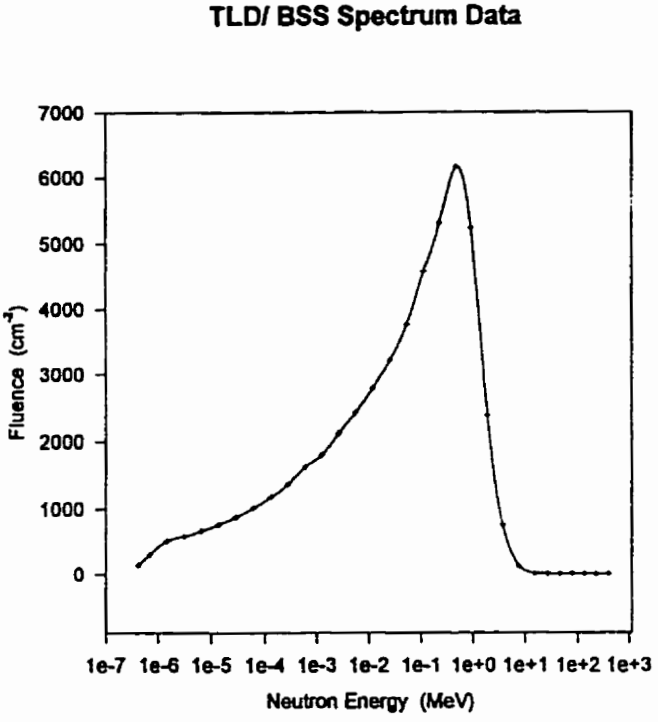

Fig. 2.4 Differential neutron energy spectrum for TLD/BSS for 15 MV [J. Liu, unpublished, 1995].

To calculate the integral ratio needed to find the total fast neutron flux, the cross-section for the (n,p) reaction in phosphorus is also needed. Price *et al* [1978] researched this topic and their graphical representation is found in figure 2.1.

It can be seen that the threshold energy is 0.7 MeV and there was an upper energy limit of 14 MeV used in the calculation of the two ratios. The integral ratios found are given in table 2.2.

The two values calculated in this thesis are comparable to the 2.89 x 10^{25} used by Price *et al* [1978] for a 25 MV x-ray beam, in previous research done with phosphorus

activation detectors. Table 2.2 shows the lack of difference found between the ratios.

Table 2.2 Integral Ratios determined for various spectra.

Spectrum	Integral Ratio found
Cf - 252	2.92×10^{25}
TLD/BSS	2.59×10^{25}
Price *et al*, [1978]	2.89×10^{25}

This small variation among the values implies that a good estimation of the fast neutron flux can be found if only an approximate differential neutron spectrum is used [Price *et al*, 1978].

The next step in this analysis is the conversion of the total flux to dose equivalence. The International Commission for Radiation Protection (ICRP) published an updated report of their conversion coefficients in 1987 [ICRP Publication #51]. The coefficients were calculated by the Monte Carlo method. Statistical uncertainties are of the order of 5%, and the overall uncertainty is cautiously judged to be within 20% [ICRP Publication #51]. The conversion coefficients used in this project are given in dose equivalent per unit fluence for monoenergetic neutrons incident in a plane parallel beam, on the principle axis, at a depth of 0.07 mm, on an ICRU sphere (a sphere made of homogeneous tissue equivalent material). The values for the coefficients varied for a neutron energy range from thermal (0.25 eV) to 20 MeV. The average conversion coefficient was found for the same range of spectrum as was used previously in the analysis (0.7 MeV to 14 MeV) using the equation,

$$CF = \frac{\int_{E_{th}}^{E_{max}} \phi_n(E)\, C(E) dE}{\int_{E_{th}}^{E_{max}} \phi_n(E) dE} \qquad (2.9)$$

where $\phi_n(E)$ is again the neutron spectrum used and C(E) is the conversion coefficient for the energy denoted. The average conversion factor (CF) calculated are given in table 2.3. The average neutron energies of the primary 18 and 15 MV beams were considered to be 2.0 and 1.8 MeV respectively and their associated conversion factors are also given in table 2.3.

Table 2.3 Calculated conversion factors [ICRP Pub. #51].

Spectrum	Conversion Factor cSv-cm^2
TLD/BSS	5.89×10^{-8}
Cf - 252	5.74×10^{-8}
2.0 MeV (monoenergetic)	5.66×10^{-8}
1.8 MeV (monoenergetic)	5.74×10^{-8}
1.5 MeV (monoenergetic)	5.84×10^{-8}

These factors are calculated solely for monoenergetic neutron beams and are given for comparison. Note that the TLD/BSS spectrum provides an underestimation of neutron energies at the isocenter because the data was taken from one meter above the x-ray target through full shielding, as if the collimators were fully closed while the detector is placed at isocenter.

2.3 Results and Observations

As shown in table 2.2 the shape of the neutron energy spectrum used for calculations has no significant effect on the determination of the fast neutron flux from activation data. The integral ratios calculated using differing spectra do not vary significantly from each other. Therefore an approximate spectrum will yield a good estimation of the true flux.

There was a surprising lack of thermal neutrons detected. This might imply that at these primary photon energies of 15 and 18 MV, there is a sufficient lack of thermal neutrons for the phosphorus activation material to register and detect. Otherwise it might indicate a need for scattering material around the detector material to provide thermalization of the neutrons from the primary x-ray beam. This is probably not the cause because in no other experimentation [Price et al, 1978; Nath et al, 1986] was extra scattering material needed. Another possibility for these results could be due to a lack of solution utilized in the liquid scintillation counter. Perhaps only using 2 ml of solution in the LSC did not allow the detection of ^{32}P activity.

The results for the 15 and 18 MV energy can be seen in figures 2.5 and 2.6 respectively, the error bars indicate a significance level of one standard deviation (σ). Errors which were not taken into account are the 20% error from the conversion factors, any error involved with the calculations of the experimental spectra and the 3% error from photonuclear interference found by Price *et al* [1978].

It can be observed in figures 2.5 and 2.6 that there is a general increase in the neutron absorbed dose equivalence as the field size increases. This does not necessarily

mean that neutron production in the treatment head increases as field size increases, in fact, neutron production is likely to remain constant as the collimators are opened [Bading *et al*, 1982]. It most likely arises from the fact that as the collimators are opened, neutrons of higher energies have a better probability of reaching the detectors (i.e. they have not yet been degraded or scattered by the collimators or shielding).

The 15 MV beam in figure 2.5 demonstrates detectable neutrons outside the primary photon beam only for two larger field sizes (20x20, 40x40 cm^2). For the 18 MV beam in figure 2.6, all four trials found detectable neutrons outside the beams up to 20 to 25 cm beyond the field edge. It must be noted that the values for neutron production outside the beam were found to be approximately one third of what was discovered in the beam.

In some of the neutron dose equivalent profiles for the 18 MV beam depressed central values were found (fig. 2.6). A flat neutron profile is expected within the primary beam. The depressed central values in some cases (20x20, 30x30, 40x40 cm^2) are within the uncertainty of a flat dose equivalent profile as expected. The 10x10 cm^2 field size indicates a depressed central value (while the other field sizes evidence a trend towards depressed central values). This is perhaps due to the geometrical design of the Varian Linacs.

At the beam edge the profile should gradually slope downwards towards a constant dose equivalent value that comes from the thermalized neutron component. Due to our lack of detection of thermal neutrons with this experiment our results only indicate a downwards slope outside the field towards a lower dose equivalent level. The detectors

are unable to detect events once the neutron energies begin to be below the energy threshold level of 0.7 MeV for P_2O_5.

Figures 2.7 and 2.8 are comparisons between the results from the two energies. The 18 MV in-beam measurements were approximately 4 times greater than the measurements for the 15 MV beam. This describes the many more energetic neutrons produced in the 18 MV beam.

It is necessary to know if our results are usable and valid. A comparison was made with computer calculated Monte Carlo simulations. The photoneutron yield was calculated by Liu *et al.*, [1997] for a Varian Clinac 2100C/2300C for photon beam energies of 10, 15, 18, and 20 MV. All of their calculations were done for a linac with the collimator jaws closed. They also determined the percent yield from each of the main components of the treatment head of these units. Therefore it is possible to calculate the photoneutron yield of a linac without the jaws. It is known that photoneutron yield increases with decreasing field size [Mao *et al.*, 1997]. Our expected yield should lie somewhere between these two values. It is possible to calculate fluence from the yield by dividing by $4\pi r^2$ (where r = 100 cm). This is based on the assumption of considering the treatment head as an isotropic neutron point source. ICRP 51 fluence to dose equivalence factors were used to convert the results. To chose the conversion factors the average primary neutron energy was needed for the locations of comparison. Kase *et al.*, [1997] determined these values using Monte Carlo computer simulations. Table 2.4 and 2.5 show the calculated results for the simulation with jaws closed and without jaws respectively.

Table 2.4 Calculated dose equivalence with jaws closed.

	18 MV (mSv/Gy)	15 MV (mSv/Gy)
Isocenter	3.55	1.93
40 cm from Iso.	3.55	1.87

Table 2.5 Calculated dose equivalence without jaws

	18 MV (mSv/Gy)	15 MV (mSv/Gy)
Isocenter	2.35	1.37
40 cm from Iso.	2.35	1.33

The reduction in the results between the two tables is due to the lack of jaws in the second calculation (table 2.5). This indicates that less neutrons are yielded because the material is no longer there in the computations to produce the neutrons through (γ,n) interactions. Since there are physically fewer neutrons in the calculations, the dose equivalence determined will accordingly be less. The expected results from our experiments using P_2O_5 should fall between these values because the jaws are only partially closed for these experiments, not entirely excluded.

Table 2.6 and 2.7 depict our P_2O_5 results found for the 18 MV and 15 MV beams respectively. Values indicate those found at the isocenter and at 40 cm from the isocenter in the patient plane.

Table 2.6 18 MV dose equivalent results for P_2O_5 (mSv/Gy).

Field Size	10x10	20x20	30x30	40x40
Isocenter	1.85 ± 0.29	2.75 ± 0.40	3.70 ± 0.52	3.06 ± 0.44
40 cm from Iso.	n/a	n/a	0.37 ± 0.11	0.45 ± 0.13

Table 2.7 15 MV dose equivalent results for P_2O_5 (mSv/Gy).

Field Size	5x5	10x10	20x20	40x40
Isocenter	0.26 ± 0.10	0.66 ± 0.16	0.73 ± 0.15	0.73 ± 0.15

As one can see the values seen at the isocenter are indeed comparable (within experimental error) at 18 MV. Sanchez *et al.*, [1989] also calculated the dose equivalent at the isocenter for a 18 MV accelerator based on experiments using a CGR Saturne 20 accelerator. They found the neutron dose to be 4 mSv/Gy. Our P_2O_5 values at 15 MV are about half of what was expected using the Monte Carlo calculations. This is probably due to the fact that the P_2O_5 results only took into account those neutrons with energies above 0.7 MeV. With an energy spectrum that has less neutrons above this limit (such as the 15 MV) it is obvious that less dose equivalence will be detected.

These results show that the P_2O_5 is a good neutron detector for higher energy beams (18 MV) and gives results approximately a factor of two less then the Monte Carlo simulation results for the 15 MV beam.

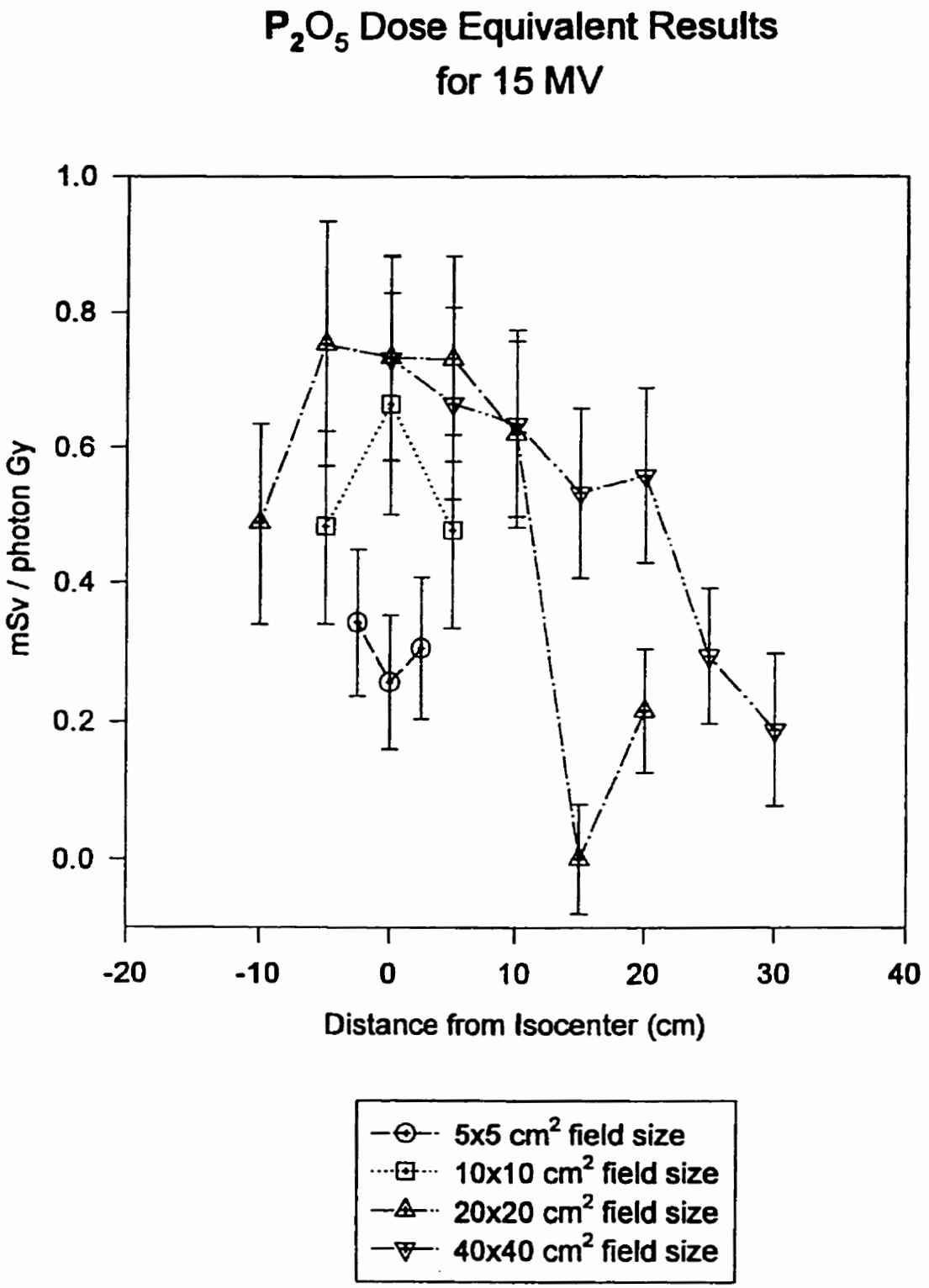

Fig. 2.5 Dose Equivalence Results for the 15 MV X-ray beam with field sizes varying from 5x5 cm^2 to 40x40 cm^2.

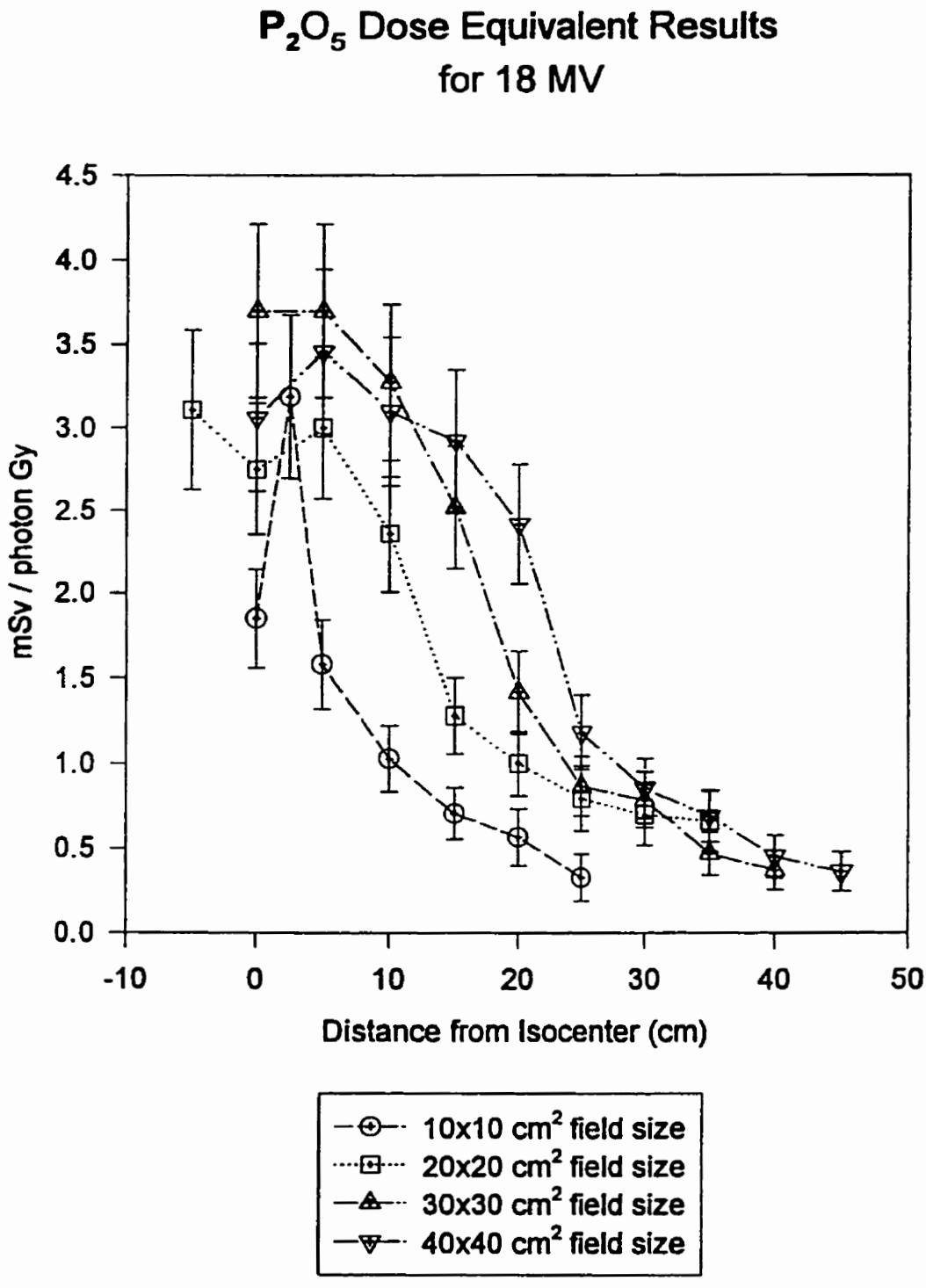

Fig. 2.6 Dose Equivalence Results for the 18 MV X-ray beam with field sizes varying from 10x10 cm^2 to 40x40 cm^2.

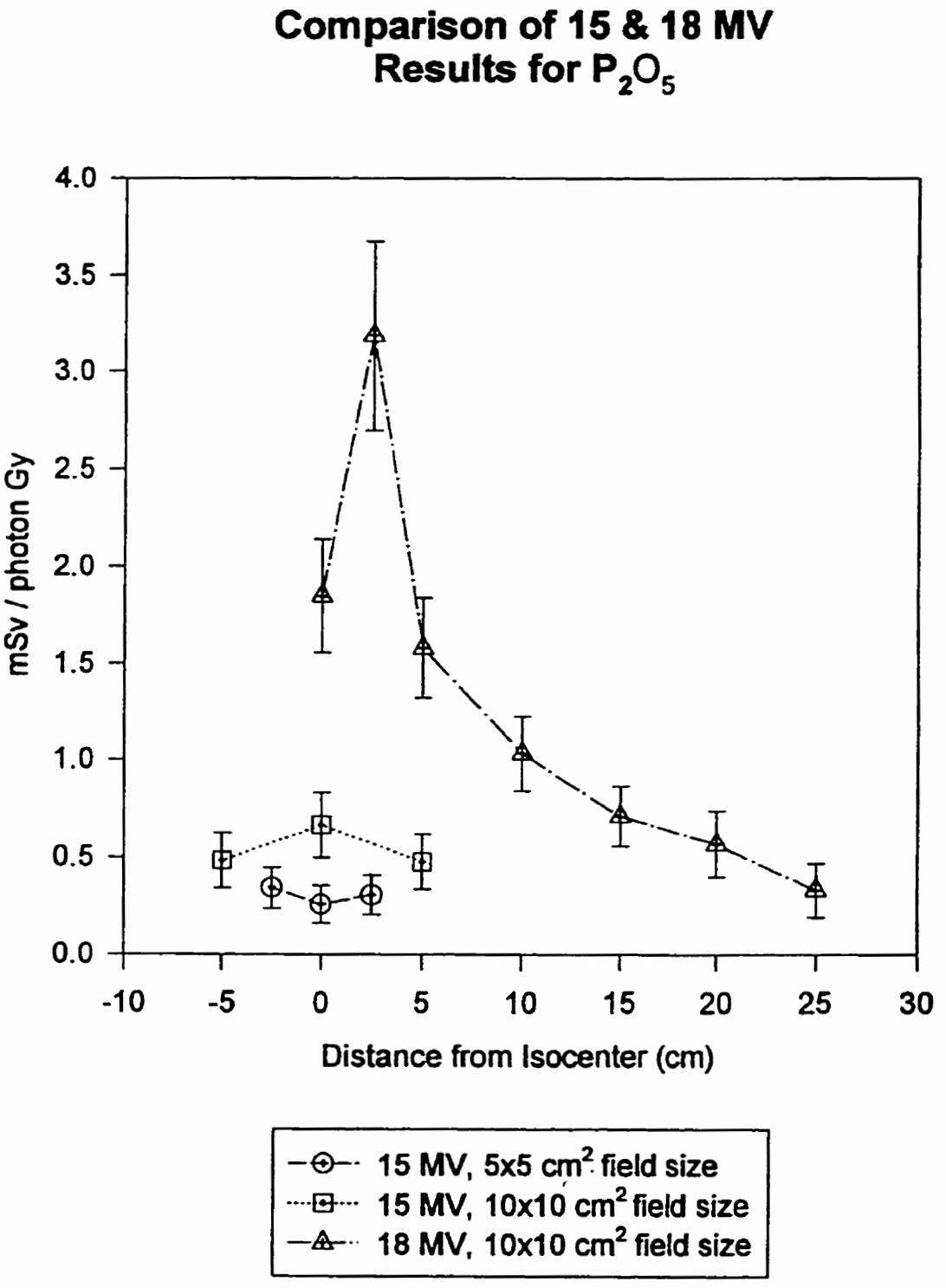

Fig. 2.7 Comparison of Dose Equivalence Results for the 15 MV (5x5 and 10x10 cm^2 field sizes) and 18 MV (10x10 cm^2 field size) X-ray beams.

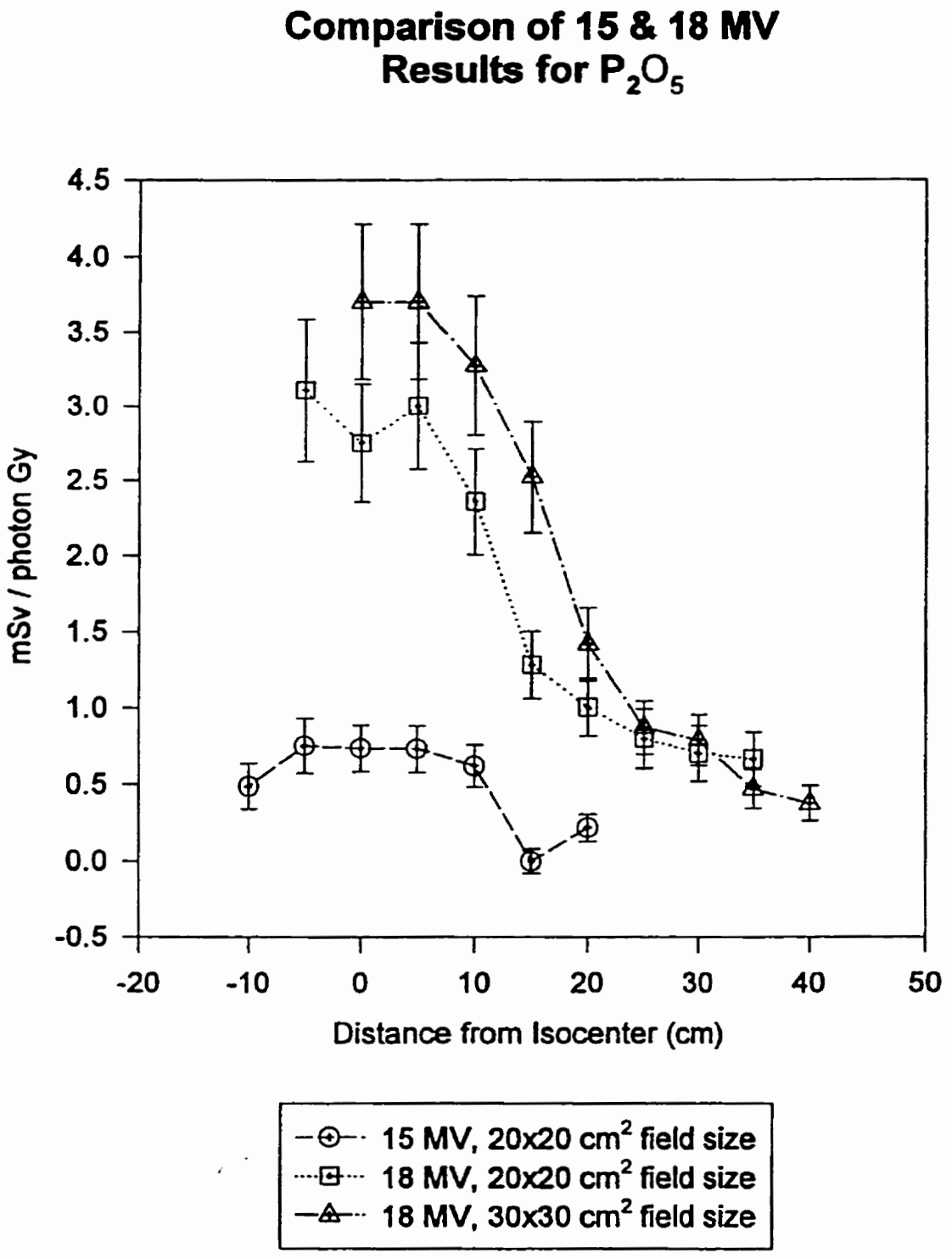

Fig. 2.8 Comparison of Dose Equivalence Results for the 15 MV (20x20 cm^2 field size) and 18 MV (20x20 and 30x30 cm^2 field sizes) X-ray beams.

Chapter 3

Experiment 2 - The Remmeter

A remmeter was used as the second method of neutron detection. This is a thermal neutron detector and is positioned within a specially designed moderator so as to give results directly in terms of dose equivalence (rem was the original dose equivalence unit). The thermal neutron detector chosen was an Indium foil neutron activation detector. This foil is made radioactive by bombardment from neutrons produced within the x-ray beam of the LINAC and its activity is then measured remotely by a gamma detector [Stephens and Smith, 1958; McCall *et al.*, 1976, 1979; Rogers and Dyk, 1981].

A neutron spectrum around a clinical medical linear accelerator consists of two main components. These are the polyenergetic spectrum of fast/slow neutrons within the primary beam, and the scattered, thermalized neutrons throughout the rest of the room. The scattered neutrons striking the concrete walls surrounding the LINAC undergo mostly elastic scattering and result in thermalized neutrons. The hydrogen in the concrete thermalizes the neutrons fairly rapidly which are then usually radiatively captured [McCall *et al.*, 1979]. Many of the neutrons may scatter back out of the walls and travel through the room several times. The result is a low energy scattered component of the neutron spectrum throughout the room. Therefore at any point in the room one can measure two components of the neutron spectrum. One is the constant thermalized or scattered spectrum and the other is the polyenergetic spectrum from the accelerator head which varies as the inverse square of the distance to the accelerator head. To understand this

concept the neutrons are assumed to be produced near the target and thus are considered an isotropic point source. The flux from the source is an ever increasing sphere which means the flux is inversely dependent on the surface area of the sphere and hence is inversely dependent on the square of the radius.

Many neutron detectors used in this situation consist of a hydrogenous moderator to thermalize fast neutrons with a thermal neutron detector inside of it [McCall *et al*, 1976]. Some examples of this type of neutron detector are; BF_3 proportional counters, Thermoluminescent Dosimeters (TLD) containing Lithium-6 or Boron-10, and activation elements. The choice for this experiment was to use activation foils made of indium and gold. These materials have a high sensitivity to thermal neutrons, and both have low energy resonances (Au-197 at 4.9 eV and In-115 at 1.46 eV) [IAEA #107, 1970]. They are used to measure slow neutrons since their neutron reaction cross sections are highest at low neutron energies. These materials demonstrate a large resonance for the (n,γ) capture reaction in the thermal energy regions. Off resonance, the cross section decreases with increasing neutron velocity which implies increasing neutron energy. Thus, in the thermal region these materials have activation cross sections that vary approximately as $1/v$, where v is the neutron velocity. Table 3.1 denotes specific characteristics of Gold and Indium. Gold has been used in previous studies as a calibration and/or comparison method for other detectors [Price *et al.*, 1978; Rogers & Dyk, 1981]. In this study gold is used to calibrate the indium foil data rather than to use in numerous trials because of its long half life of 2.7 days. The decay time needed for Gold between consecutive trials delays data gathering excessively. Thus an indium foil using the $^{115}In(n,\gamma)^{116m}In$ reaction

with a half life of 54.12 minutes is used to take data, and the gold foil is used only for calibration of the indium foil. Gold and indium also have a low probability for photon

Table 3.1. Characteristics of the activation materials - gold and indium [Knoll, 1989].

	Isotope Abundance	Cross section ($x10^{-28}$ m^2)	Reaction Product	Half Life $\tau_{1/2}$
Indium	^{113}In (4.23%)	56 ± 12	^{114m}In	49 days
		2.0 ± 0.6	^{114}In	72 sec
	^{115}In (95.77%)	160 ± 2	^{116m}In	54.12 min
		42 ± 1	^{116}In	14.1 sec
Gold	^{197}Au (100%)	98.5 ± 0.4	^{198}Au	2.695 days

induced reactions which makes them ideal for measurements in and around high energy x-ray beams.

Hydrogenous moderators are used to accompany thermal neutron detectors because hydrogen, being approximately equal in size to a neutron, can effectively thermalize fast (high energy) neutrons through elastic scattering collisions. An incident neutron can transfer all of its energy in a single collision with a hydrogen nucleus, whereas only a small fraction of energy is transferred in a collision with larger, heavier nuclei. Thus a moderator attempts to slow down high energy neutrons through collisions with hydrogen so the activation foil within the moderator will be able to detect these thermalized neutrons.

In 1960, during an attempt to discover a useful neutron spectrometer, Bramblett, Ewing and Bonner placed a small lithium iodide scintillator in a series of polyethylene

moderators of differing diameters. They discovered that a moderating polyethylene sphere with a diameter of 12" has a similar response function to the dose equivalence delivered per neutron as a function of energy. Figure 3.1 depicts the response curves of various diameter moderators. The 12" diameter polyethylene moderator provided a close approximation of neutron dose equivalence. For moderator diameters greater than 12 inches too many of the slower neutrons were lost (scattered out), and for thinner diameters of less than 12 inches, too many of the fast neutrons were not thermalized and

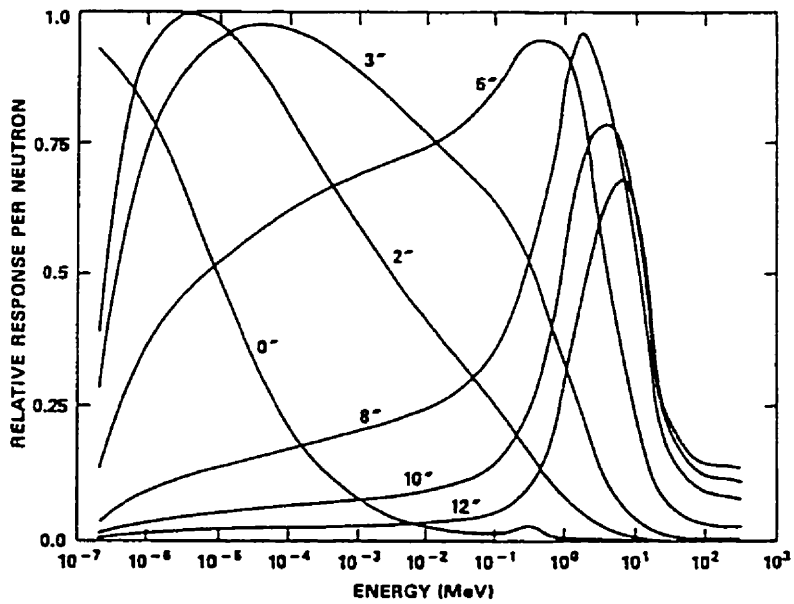

Fig. 3.1 Response curves of moderators of varying diameters.

thus were unable to be captured by the thermal neutron detector at the center of the moderator. The relationship uncovered was coincidental but highly advantageous. It allows for a specially designed moderator in conjunction with a thermal neutron detector to give dose equivalence readings directly. The spherical geometry of the moderator

allows for a relatively non-directional detector response. The moderator utilized for this project is cylindrical and therefore care must be taken as to which side faces the primary x-ray beam.

McCall *et al.* [1979] describes the neutron dose around medical electron accelerators as having neutrons with energies between 100 keV and 2 MeV. In this energy region most remmeter responses accurately reflect the dose equivalence of the neutron spectrum [Rogers and Dyk, 1981].

This technique is limited by uncertainties and errors normally associated with remmeters and calculations of dose equivalence. One restriction of this method is that the detector gives the dose equivalence and not the neutron spectrum. In order to calculate the absorbed dose or fluence an accepted neutron spectrum must be assumed. A second restriction for this technique is the production of photoneutrons within the moderator when placed within the primary beam [Rogers and Dyk, 1981]. Polyethylene is composed of mainly hydrogen and carbon. The cross section for photoneutron production in carbon has a resonance (or peak probability of occurrance) between 20 and 25 MeV [IAEA #156,1974], implying photoneutron production can occur for higher energy x-ray beams. Estimates have shown that this effect can be significant [Rogers and Dyk, 1981]. A third disadvantage with remmeter type moderators is the specific design required. The remmeter can be very complicated to build and usually demands the purchase of one commercially built.

After irradiation of the foil-moderator set up the second part of the experiment requires the use of a second detector to determine the induced activity in the gold and

indium foils. Because the activation foils used in this experiment are both gamma emitters, a gamma ray detector was used. A high purity (or intrinsic) germanium (HPGe) semiconductor detector was chosen because it has the best energy resolution of the gamma ray detectors available. This is due in part to the fact that the density of a solid gamma detector is a 1000 times greater than the density of a gas detector. This means that there is a larger number of carriers for any given incident radiation event. The information carriers in a semiconductor detector are electron-hole pairs, (which are analogous to the ion pair created in a gas filled proportional counter). These carriers are created by the ionizing charged particle as it moves through the detector (the particle can be primary or secondary radiation). In an intrinsic germanium detector 3 eV are required to produce one 'electron-hole' pair. The motion of these 'electron-hole' pairs in the detector produces the basic electrical signal received.

The detector used for this project was a p-type coaxial HPGe. The outside of the crystal has a small (on the order of microns) layer of heavily doped n^+, which is the rectifying contact of the detector. The inside of the coaxial crystal is the p^+ side electrode which is considered to be the blocking contact. The current from the created electron-hole pair is then detected at the contacts by a resistor and then the signal is passed on to the preamplifier.

Due to the small bandgap (0.7 eV) for germanium, the detector must be housed within a vacuum tight cryostat to prevent thermal conductivity between the crystal and the surrounding air. The cryostat must also be cooled to 77 Kelvin with liquid nitrogen to further inhibit thermally induced leakage current. The preamplifier is usually located close

to the cryostat housing so as to minimize capacitance.

A schematic of our detector system is shown in figure 3.2. It can be seen that the preamplifier is not just an impedance matcher but is also a means to supply the bias voltage to the detector. The linear amplifier is responsible for pulse shaping and amplitude gain, while the multichannel analyzer sorts successive signal pulses into parallel amplitude channels.

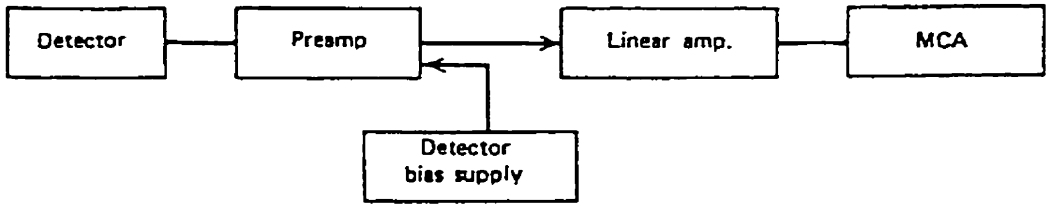

Fig. 3.2 High Purity Germanium Detector System Schematic.

3.1 Methods & Materials

The absolute efficiency is defined as the number of pulses measured over the number of radiation quanta emitted by the source. This efficiency takes into account the source detector distance, and thus the solid angle. The intrinsic efficiency does not depend on the solid angle and is the ratio of the number of pulses measured over the number of quanta incident on the detector. The absolute efficiency for this detector was found using a calibrated Co-60 source with a known activity and this was counted with our gamma detector. The ratio of counts detected over the number of counts emitted, which is the absolute efficiency was determined to be 0.48 %, using Co-60 1332 keV full

energy peak.

Energy resolution of a detector reflects the ability to resolve the difference between two energy peaks. The pulse height distribution around an average pulse height is what gives the quality of good verses bad resolution. If the width of the distribution or the Full Width at Half Maximum (FWHM) height, is large compared with the pulse height the resolution is poor. In other words,

$$Resolution\ R = \frac{FWHM}{H_o} \tag{3.1}$$

where H_0 is the peak centroid for the energy being measured. For the detector used the smaller the resolution ratio R the better the detector resolution. For gaussian shaped peaks with standard deviation σ, the FWHM is 2.35σ. Factors that contribute to poor resolution are the effects of carrier statistics, charge carrier collection and electronic noise. The resolution found for the HPGe used in this project was 0.2% (or approximately 2 keV) at 1332 keV (Co-60).

After a detector observes an 'event' it takes a finite amount of time for the detector to recover and be able to count another event. This recovery period is called the dead time, τ. The total amount of dead time must be measured since it is a source of error for high counting rates. Further, there are two classes of dead time: paralyzable, and non paralyzable.

For non paralyzable dead time, the detector essentially shuts off and ignores any inputs until τ has passed. Paralyzable dead time involves events which occur during the

dead time τ. If an event occurs before τ is up, the clock starts again without adding this new event to the tally of 'events'. Thus, the detector is essentially off until a full time period τ has elapsed since the last event has occurred. Most counting systems have a combination of these two dead time effects. The dead time for the HPGe detector used in this project was measured using the 'two source' method. The count rate from two Cesium-137 sources was found individually and in combination. The calculated dead time was found to be 2.44 % using the following equation,

$$\tau \qquad \frac{m_1 m_2 - [\, m_1 m_2 (m_{12} - m_1)(m_{12} - m_2)\,]^{1/2}}{m_1 m_2 m_{12}} \tag{3.2}$$

where m_1, m_2, and m_{12} are the observed count rates for source 1, source 2, and the combined sources respectively. These losses are small enough so they do not affect the distribution of counts very much in the present work.

The foils used in this thesis were composed of Indium and Gold and were purchased from Reactor Experiments Incorporated+. Some of their characteristics can be found in table 3.2. The moderator used in this experiment was purchased from Victoreen Inc.++

The experimental variables were: 1. the field size (20x20, 40x40 cm^2), 2. the location of the detector with respect to the isocenter (isocenter, 15cm from field edge), and 3. the beam energy (15 and 18 MV). Without the moderator it can be assumed that

+ Reactor Experiments Inc., Sunnyvale, CA.
++ Victoreen Inc., Cleveland, Ohio.

Table 3.2 Gold and Indium foil information.

Nuclear Reaction	$E_{resonance}$	Diameter	Thickness	Density
$In^{115}(n,\gamma)In^{116m}$	1.458 eV	4.4 cm	0.127 mm	7.28 g/cc
$Au^{197}(n,\gamma)Au^{198}$	4.9 eV	4.4 cm	0.025 mm	19.3 g/cc

the foils would measure the constant thermalized neutrons scattered from the concrete room walls. Within the beam, bare gold and indium foils are susceptible to photoneutron production within them [IAEA #156, 1974]. With the moderator the dose equivalence of the neutrons produced by the LINAC would be measured. 4000 Monitor units were given at a dose rate of 600 monitor units per minute. The detector was placed within the primary beam and outside of it. Within the primary beam some photoneutron production in the moderator might take place, though at the energy levels this project is using it should not make a significant difference. The results are expected to be comparable to the phosphorous detector results.

Once the indium foil was irradiated it was placed in front of the HPGe detector after a waiting period of approximately 30 minutes to one hour. During this time the activity of the Indium-114, Indium-116, and the induced radioactivity in the aluminum foil backing becomes insignificant. The energy calibration of the HPGe detector was done with Ba-133 (356 keV), Cs-137 (662 keV), and Co-60 (1173 and 1332 keV). The irradiated foil was counted for approximately 30 minutes, with the region of interest at the 1294 keV peak. Once a count rate was found then a saturation count rate was calculated using a similar formula to equation 2.6,

$$C_s = \frac{C_t(\lambda t_c)\exp(\lambda t_w)}{[1-\exp(-\lambda t_i)][1-\exp(-\lambda t_c)]} \quad (3.3)$$

where C_t is the count rate found, λ is the decay constant for indium, t_w,t_i and t_c are the waiting, irradiation and counting times respectively. The saturation activity of the foil was computed using the following formula,

$$A_s = \frac{C_s}{eNf} \quad (3.4)$$

where A_s is the saturation activity found, e is the gamma counting efficiency of the detector (for that particular peak), N is the number of target nuclei in the sample, and f is the branching intensity for the peak being looked at (further information can be found in table 3.3).

Table 3.3 Saturation activity information for the foils.

	N (target atoms)	Peak energy	e	f
Gold	2.23×10^{21}	411 keV	0.0225	0.99
Indium	7.06×10^{21}	1294 keV	0.0050	0.844

The number of target atoms is calculated using equation 2.2 again,

$$N = (N_A mma) / A \quad (3.5)$$

where N_A is avogadro's number, m is the mass of the foil, n is the number of target atoms in one molecule of activation material, a is the fractional natural abundance and A being the molecular weight.

To determine the neutron dose equivalence from the induced activity in the activation foil, a calibration of the moderator and activation detector system is required using a neutron source of known activity. Rogers and Dyk [1981] have determined the calibration factor for a similar moderator and Gold foil system (as in the present experiment). Thus a Gold foil and moderator combined was used to calibrate the Indium foil and moderator combination. Once the saturation activity of the Gold foil is found it can be used to find R, the ratio of the saturation activities for the same location and beam energy (see table 3.4).

Table 3.4 Saturation activity ratio.

	15 MV	18 MV
Ratio (R)	0.132	0.129

Then all the indium saturation activities can be calibrated by multiplying them by the respective ratio needed.

The next step is to determine the dose equivalence using the formula by Rogers and Dyk [1981],

$$D.E. = A_s \times 4.07 \times 10^{23} \ (mrem / Bq \ per \ target \ nuclei) \qquad (3.6)$$

where the mrem will be converted to sieverts. (mrem = 10^{-5} sieverts)

3.2 Results and Discussion

As expected the data depicted a marked increase in dose equivalence inside the primary x-ray beam compared with the results seen outside the beam for each field size. The standard deviation from the number of counts recorded by the HPGe detector can be considered negligible compared with the results obtained, being roughly four orders of magnitude smaller than the calculated results. Figures 3.3 and 3.4 show the spectra obtained by the HPGe detector from the indium and gold foils respectively.

It can be seen in figures 3.5 and 3.6 that when the remmeter is placed at the isocenter with a 0x0 cm^2 field size (i.e. with the collimator jaws closed) the dose equivalence detected is approximately half of what is detected when the remmeter is placed at isocenter with the collimator jaws open to a 20x20 or 40x40 cm^2 field size. Fewer neutrons are being detected because either their energy is being degraded by the collimators or they are being scattered away.

The same figures show a slight decrease in dose equivalence from the 20x20 cm^2 field size to the 40x40 cm^2 for the detectors placed 15 cm outside the x-ray beam edge. 15 cm from the beam edge implies that the detector is 25 cm from the isocenter for the 20x20 cm^2 field size and is 35 cm from the isocenter for the 40x40 cm^2 field size. This could be due to statistical error of the results but more trials would have to be taken to be

completely sure. Another theory on the decrease in dose equivalence could be due to the position of the detector. In order to place the detector outside the field for the 40x40 cm^2 it must be moved another 10 cm away from the isocenter (thus it is now 35 cm away from the central axis rather than 25 cm). This increase in distance might mean that even though the neutron flux would be the same, the dose equivalence would not because more of the received neutrons would have energy degradation due to the shielding around the x-ray target. However this does not explain why the same decrease in dose equivalence is happening when the detector is kept within the primary beam.

As expected more neutrons are produced in the 18 MV beam than in the 15 MV beam. This can be seen in figure 3.7 which compares both energies for the same positions of the detector. The 18 MV beam produced approximately twice the number of neutrons as the 15 MV beam.

Qualitatively the results were as they should have been, however quantitatively the results are approximately 3 orders of magnitude greater than the results obtained with the P_2O_5 experiment. This data implies that exposures of this type could be very dangerous due to the extra dose involved. Of course we realize through the work with Monte Carlo simulations and other detectors that this is not the case since the expected dose equivalence is approximately 1000 times less. Thus there must be something wrong with either the experimental method or with the calculations used to achieve the solutions. Various aspects of the setup and computations were addressed to determine the error.

The quality factors of neutrons have been changed since the conversion factors were last used [Nath *et al*, 1986] but the quality factor only changed by a factor of two.

This change is not expected to propagate to produce such a large error. Also the number of trials for all the experiments should be increased but again this does not explain the numerical difference between the remmeter results and P_2O_5 detector data. Another issue of contention might be the differing size of the gold foil used for this project compared with the one used by Rogers and Dyk [1981], though the difference is slight. Their foil is half the diameter of the gold foil used and the same thickness as the indium foil used for this project. The surface area of our foils (and thus the number of target nuclei seen at the foil surface) are four times the size of the foil used by Rogers and Dyk. Again this difference is not enough to account for the discrepancy found in our results. There is obviously a systematic error involved with this experiment. It was suspected that the conversion factor (140 mrem/(photons/s) per g) sited in a previous paper [Rogers and Dyk, 1981] could be in error.

Our results using Rogers and Dyk's [1981] conversion factor are a magnitude of 1000 higher than expected. The P_2O_5 experiment has been proven reliable for the 18 MV beam and results are within a factor of two for the 15 MV beam. It was decided to use the P_2O_5 as the standard by which to compare our foil saturation activity results. Table 3.4 shows our values for the saturation activity.

Table 3.4 Saturation Activities of Indium foils (dis/sec/target nuclei ($x10^{-15}$))

Energy	Field Size	0x0 cm^2	20x20 cm^2	40x40 cm^2
18 MV	Isocenter	3.08 ± 0.62	4.46 ± 0.68	2.76 ± 0.05
	35 cm from Iso.		5.25 ± 0.08	2.49 ± 0.11
15 MV	Isocenter	2.64 ± 0.02	1.57 ± 0.01	1.33 ± 0.10
	25 cm from Iso.		1.02 ± 0.01	1.65 ± 0.40

The statistical error from the detected counts is negligible (less than 1%). The error seen in these tables is from the variability of the determined saturation activity between trials. This error is large (approximately 20%) for 3 values (at the isocenter for the 0x0 and 20x20 cm^2 field sizes - 18 MV, and 35 cm from the isocenter for the 40x40 cm^2 field size - 15 MV).

The saturation activity of the 20x20 cm^2 field size (isocenter) for the 18 MV beam was used to compare with the P_2O_5 dose equivalent (mSv/Gy) found for the same variables. The ratio of the two values was then multiplied by all of the saturation activities found. The results are shown in table 3.5. The ratio found was 6.166×10^{14} mSv/Gy per dis/sec/target nuclei.

Table 3.5 Dose Equivalence (mSv/Gy) using P_2O_5 (18 MV, 20x20, Iso.) as a standard.

Energy	Field Size	0x0 cm^2	20x20 cm^2	40x40 cm^2
18 MV	Isocenter	1.90 ± 0.38	2.75 ± 0.42	1.70 ± 0.03
	25 cm from Iso.		3.24 ± 0.05	1.54 ± 0.07
15 MV	Isocenter	1.63 ± 0.01	0.97 ± 0.01	0.82 ± 0.06
	35 cm from Iso.		0.63 ± 0.01	1.02 ± 0.25

As can be seen from the above table these results do not coincide with values given by either the P_2O_5 (tables 2.4 and 2.5) or the calculated Monte Carlo computer simulations (tables 2.6 and 2.7). Table 3.6 gives the results for the Indium foil if a P_2O_5 standard from each field size is used to determine the dose equivalent results. Comparison of these results with Monte Carlo simulations and the P_2O_5 seems to be in agreement (within experimental error) except for the 20x20 cm^2 field size for the 15 MV beam, though it is within a factor of two of the P_2O_5 results. The 0x0 cm^2 field size results for the Indium foil are within experimental error for the Monte Carlo calculated results.

Table 3.6 Dose Equivalence (mSv/Gy) using P_2O_5 (18 MV, ea field size, Iso.) as standards.

Energy	Field Size	0x0 cm^2	20x20 cm^2	40x40 cm^2
18 MV	Isocenter	3.55 ± 0.71	2.75 ± 0.42	3.06 ± 0.06
	25 cm from Iso.		3.24 ± 0.05	2.76 ± 0.12
15 MV	Isocenter	3.04 ± 0.02	0.97 ± 0.01	1.47 ± 0.11
	35 cm from Iso.		0.63 ± 0.01	1.83 ± 0.44

The remmeter should be calibrated with a known neutron source to calculate a conversion factor but lacking this a comparison with reliable experimental results can be done and was done in this case. These results indicate the need for a conversion factor for each field size used in the experiments.

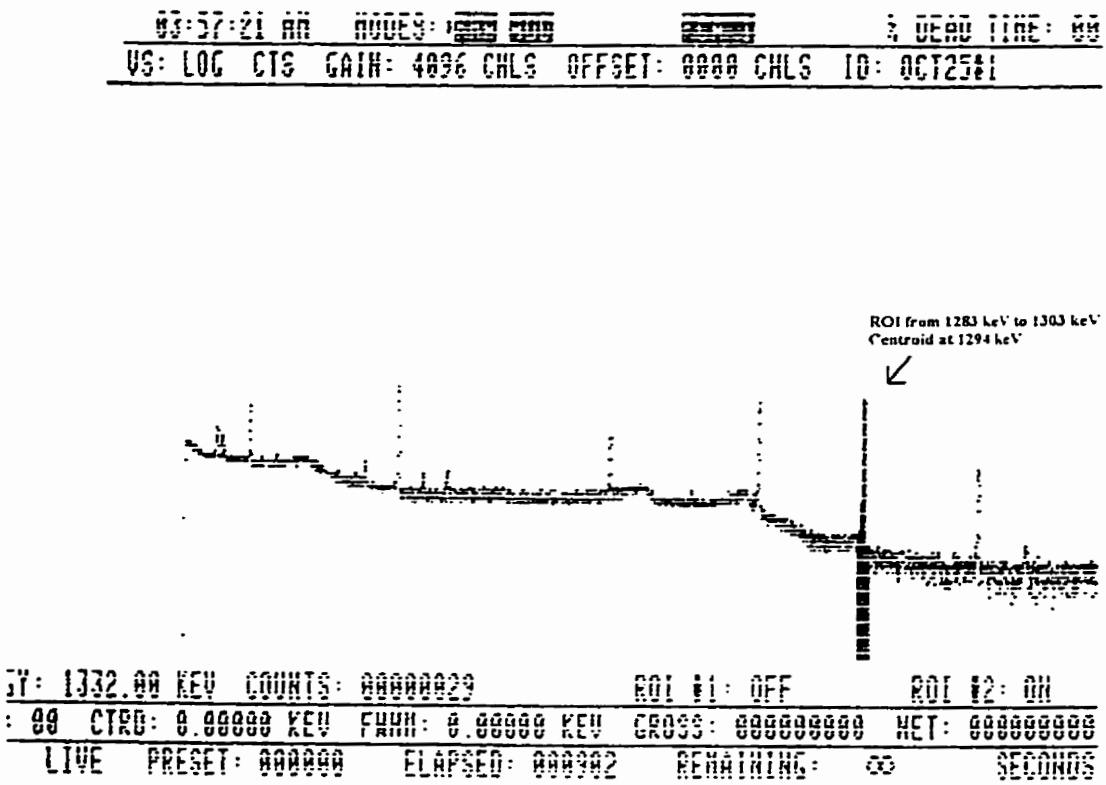

Fig. 3.3 Spectra obtained from the HPGe detector for the Indium foil.

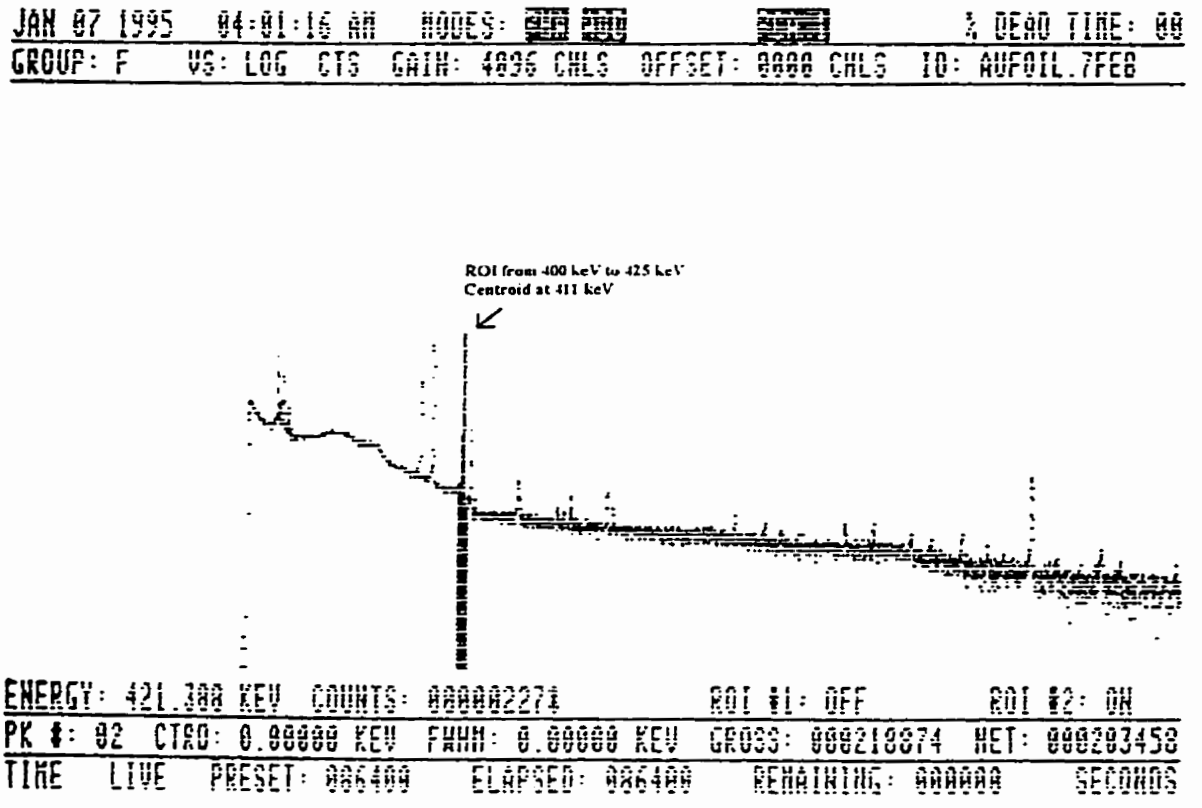

Fig. 3.4 Spectra obtained from the HPGe detector for the Gold foil.

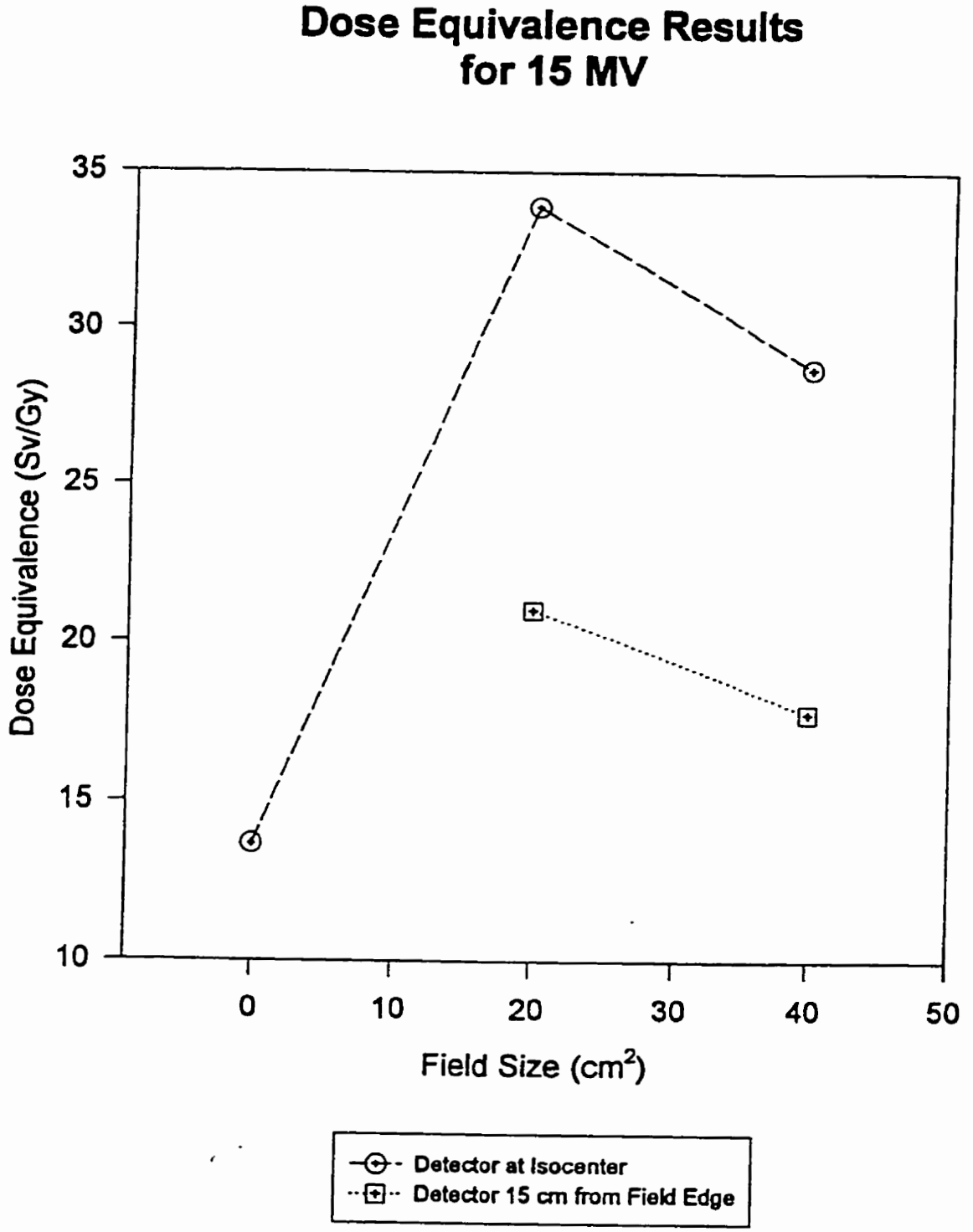

Fig. 3.5 Dose Equivalence Results for the 15 MV X-ray beam at the Isocenter and 15 cm from the field edge.

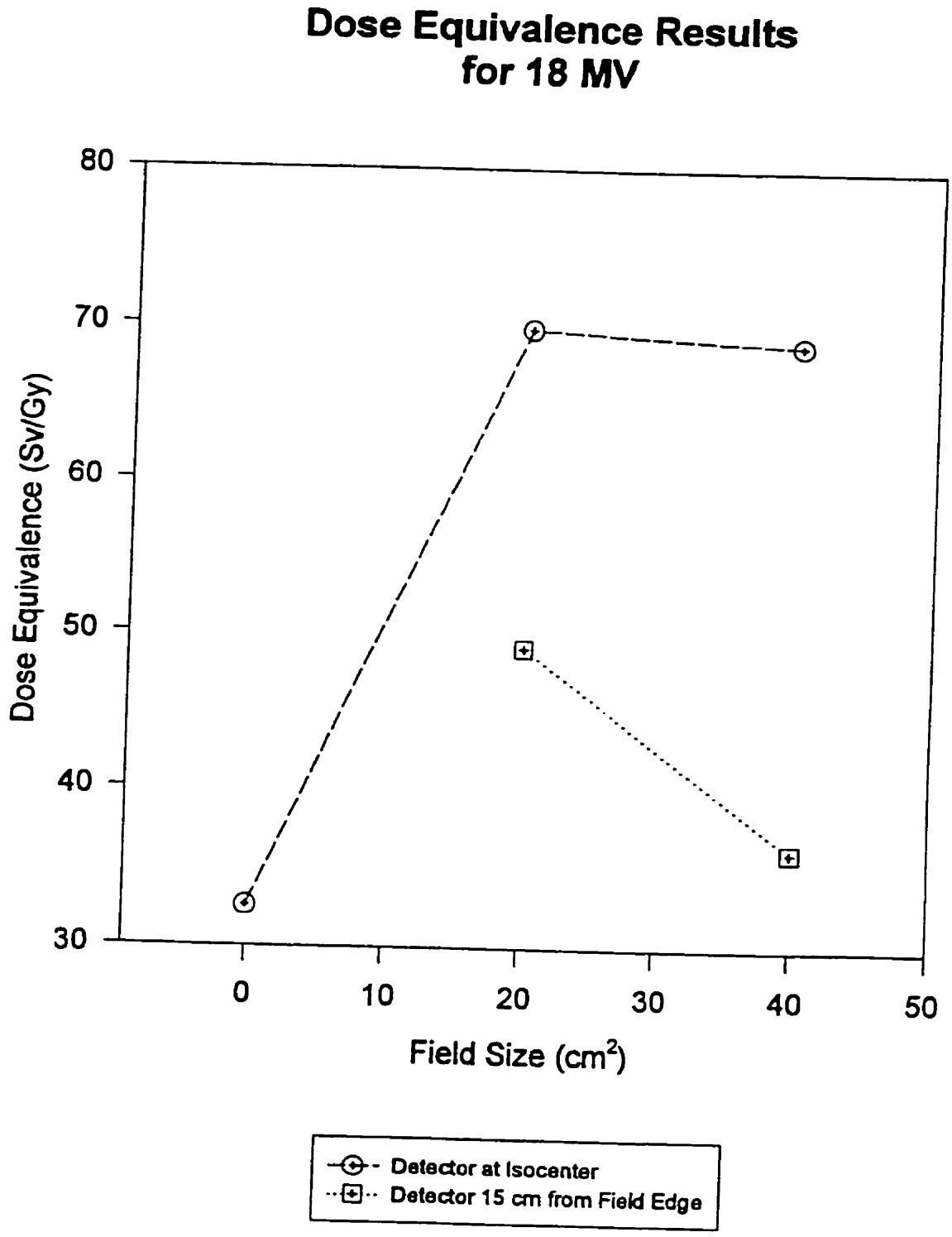

Fig. 3.6 Dose Equivalence Results for the 18 MV X-ray beam at the Isocenter and 15 cm from the field edge.

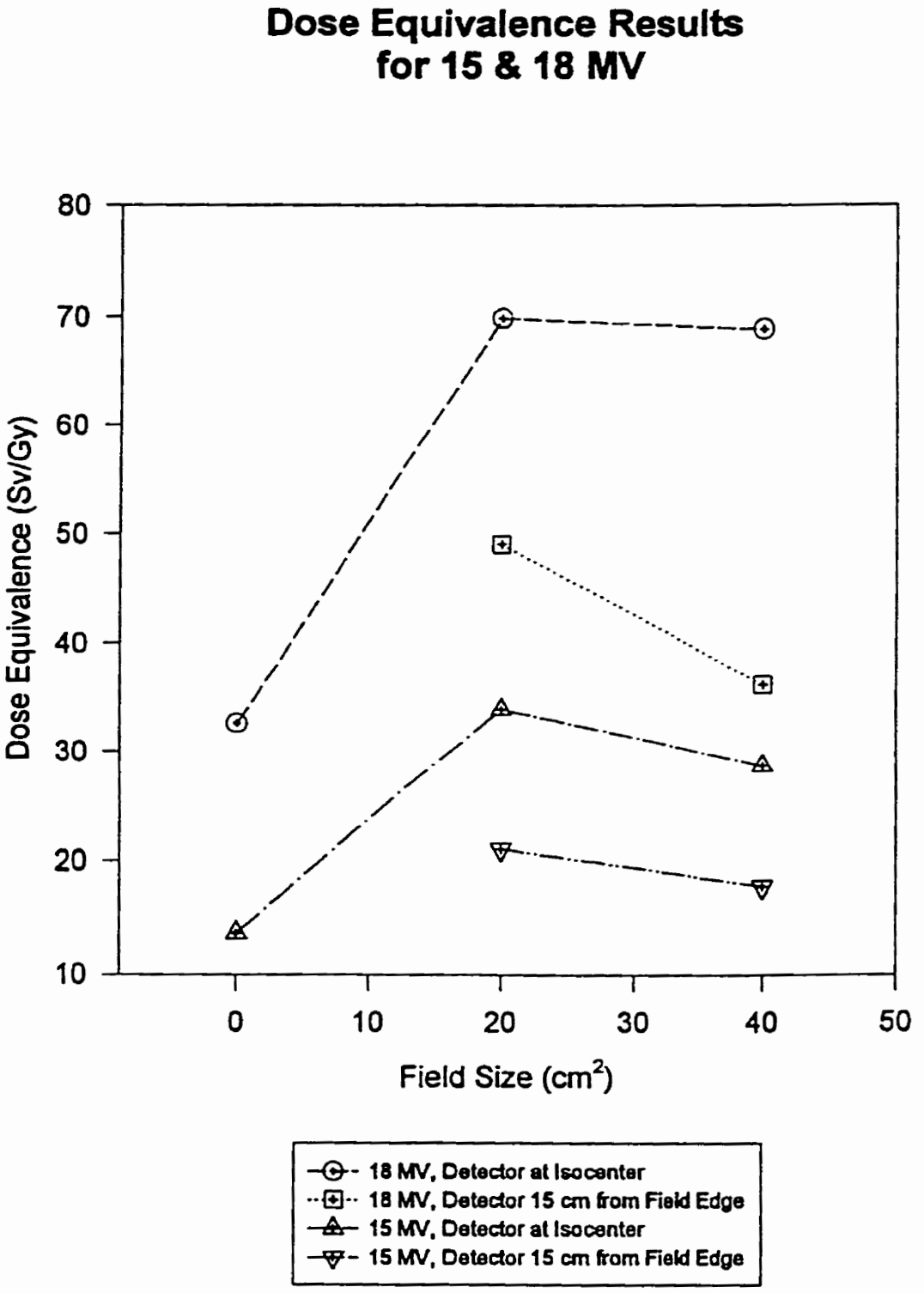

Fig. 3.7 Comparison of Dose Equivalence Results for the 15 and 18 MV X-ray beams (at the Isocenter and 15 cm from the field edge).

Chapter 4

Experiment 3 - Superheated Drop Detectors

Superheated Drop Detectors (SDD) are a fairly recent introduction by R.E. Apfel who holds the patent (U.S. 4 143 274) for them. This project has considered their use as neutron dosimeters. The SDD is a vial of gel containing thousands of superheated droplets that expand upon neutron-induced vaporization. It is based upon the principle of the bubble chamber; namely the initiation of vapour bubbles by energetic ions in superheated liquids [Apfel, 1979]. Thus each drop in the SDD is a continuously sensitive, miniature bubble chamber [Roy *et al*, 1987]. While other detection techniques are expensive and labour intensive, the SDD is purported to be inexpensive, easy to use, and can be read directly in dose equivalent units [Nath *et al*, 1993; Apfel, 1979; Roy *et al*, 1987].

The theory of the SDD originates with the Bubble chamber, which was invented in 1952 by D.A. Glaser [Henderson, 1970]. A bubble chamber holds a liquid far above its normal boiling point but which is held quiescent by an externally applied pressure. Upon release of the external pressure the liquid becomes superheated. Boiling occurs with fluctuations of high energy density. These are produced by either thermal fluctuations that produce momentary holes in the liquid, or the fluctuations are produced along the ionized track of a charged particle. The nuclear event is then recorded by the trail of bubbles nucleated by elementary particles. The chamber is rendered stable again by

repressurization.

This new neutron detector has superheated droplets suspended in a host gel or polymer. The subdivision of the liquid into droplets assures that one nucleation event does not consume the whole sample, thus the repressurization of a chamber is not needed. The liquid can be introduced into the gel at a temperature below its boiling point and the temperature can slowly be raised to room temperature, or the liquid can be introduced at a pressure greater than vapour pressure and then the pressure can slowly be lowered to atmospheric pressure. There is no need of a power source with these detectors because radiation triggers the release of the stored mechanical energy in the superheated droplets.

4.1 Theory

When a liquid is in the region of temperature and pressure belonging to the gaseous state and yet still has the characteristics of the liquid phase the liquid is in a metastable state and is defined as being superheated. In this state the vaporization of the droplets is influenced by how much ionization is produced by the neutrons and where it is produced. Also the vapourization is influenced by the thermodynamics of the processes resulting in a microscopic bubble.

Fast neutrons can create ionization from the elastic recoil nuclei produced after an interaction within a drop. Ionization can also occur from charged particles produced when a neutron induces a nuclear reaction of sufficiently high Q value. In this way thermal, as well as fast, neutrons can also be detected.

The theory of neutron-induced nucleation of superheated drops involves three concepts: 1. neutron-nucleus interaction which is the realm of nuclear physics, 2. interaction of ions with matter, which entails atomic physics, and 3. dynamic processes resulting in a microscopic vapour bubble, which involves the theory of fluids and thermodynamics. Thus it is not surprising that there is no existing theory which is capable of making accurate, exact estimates of, for example, the threshold energy required to nucleate bubbles in a given liquid superheated to a known degree [Roy *et al*, 1987].

The maximum energy a nucleus can receive from a neutron occurs in a head-on elastic collision,

$$E_{max} = \frac{4A\,E_n}{(A+1)^2} \qquad (4.1)$$

where A is the atomic weight in amu of the nucleus [Apfel, 1979]. When the nucleus is struck by a neutron the nucleus is ejected from its electrons and proceeds to deposit its energy through the liquid until electron collisions and charge capture bring it to rest. It is possible that different nuclei will receive different amounts of energy from the incident neutron. The superheated liquids used for these detectors are halocarbons (halogens such as chlorine and fluorine bonded to carbons). The refrigerant Freon 12 (CCl_2F_2) is the liquid used in our detectors and it has a boiling point of approximately -28.5 degrees celsius. The nucleus that has the major role in bubble vaporization is determined by the ion that has the highest LET within the liquid.

A bubble of radius r, possesses an effective surface pressure of, $2\gamma(T)/r$ where $\gamma(T)$ is the surface tension of the liquid at temperature T. The surface pressure is balanced

by the difference between the pressure in liquid and that of the vapour in the bubble [Roy *et al*, 1987] thus,

$$\frac{2\gamma(T)}{r} = P_v(T) - P_o = \Delta P \tag{4.2}$$

where P_o is the external pressure (the pressure of the liquid and thus, the atmospheric pressure). Roy *et al.* [1987] showed that the critical radius required to attain a stable vapour bubble, r_c, is given by;

$$r_c = \frac{2\gamma(T)}{\Delta P} \tag{4.3}$$

The free energy to from a bubble of radius r can be found using,

$$\Delta = 4\Pi r^2\gamma - \frac{4}{3}\Pi r^3(\Delta P) \tag{4.4}$$

where the pressure difference multiplied by the volume of the bubble is subtracted from the surface tension, γ, multiplied by the surface area of the bubble [Roy *et al*, 1987]. This equation indicates that the reaction will proceed spontaneously if the pressure difference component is larger than the surface tension component (i.e., if the free energy is negative). Both equation 4.4 and 4.3 imply that as the pressure difference increases (or as the degree of superheat of a given liquid increases) the critical radius needed for bubble

creation decreases. This means that less energy is required to nucleate a vapour bubble [Roy *et al*, 1987].

The model that best describes the bubble nucleation mechanism has been agreed to be F. Seitz's 'thermal spike' [Apfel *et al*, 1979]. This approach suggests that ions deposit energy locally, which is equivalent to a hot spot that literally explodes (due to sudden heat deposit), creating vapour nuclei of critical size. The energy deposited along the ion's path in the medium, corresponding to twice the critical radius of the liquid, will be the energy that will contribute significantly to bubble formation. Vapour nucleation is a very inefficient process [Roy *et al*, 1987] with only four to six per cent of the energy deposited being effective in bubble nucleation.

Freon 12 has a boiling point of -28.5 degrees celsius and is sensitive to thermal neutrons as well as fast neutrons at ambient temperature and pressure. This sensitivity of Freon 12 to thermal neutrons cannot be explained by the elastic head-on collision mechanism discussed previously. Roy et al [1987] calculated that the minimum energy needed by a neutron, at 10 degrees celsius, to form a vapour bubble of critical radius is 1.2 keV, whereas thermal energies are three orders of magnitudes smaller than this fundamental energy. Thus it was concluded that the sensitivity of Freon 12 was due to the following nuclear reaction;

$$^{35}_{17}Cl + {}^{1}_{0}n \rightarrow {}^{35}_{16}S + {}^{1}_{1}H\ (598\ keV)$$

The sulphur ion deposits its entire 17 keV in a range typically less than one critical

radius. The proton (598 keV) deposits only a small fraction of its energy within the critical radius.

The relative response of the Freon 12 - SDD was compared to the ICRP recommended 'ideal dosimeter' dose equivalence response curve [Apfel and Lo, 1989]. Figure 4.1 depicts the relationship between the two response curves. The Freon 12 - SDD response has been normalized at 1 MeV to the ICRP response. It can be noted that both responses follow the same trend to within a factor of 10 below 100 keV and to within 40% above 100 keV [Apfel and Lo, 1989]. This indicates that it is possible to create a rem-response neutron dosimeter The probability of interaction is proportional to the volume of the liquid; the volume of vapour evolved from radiation induced interaction is an integrated measure of the radiation dose.

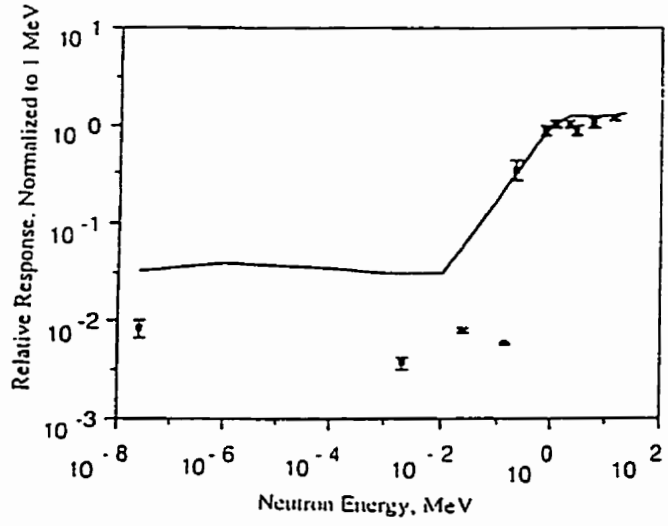

Fig 4.1 Relative comparison of the SDD response (squares) verses ICRP recommended dose equivalence curve (solid line).

4.2 Methods & Materials

Neutrometer-HD™, purchased from Apfel Enterprises Inc.[+] was the SDD used for this project. It has thousands of droplets (approximately 20 000) of Freon 12 suspended in a gel contained in a 4 cm^3 vial. A graduated pipette is fitted onto the vial. The drops expand from roughly 65 to 500 μm, and the expansion of the bubbles displaces the gel into the pipette. The volume displaced is equated with dose equivalence by the equation,

$$DE\,(mSv) = C_1 \ln[1 - volume\,(cm^3) / C_2] \qquad (4.5)$$

where C_1 and C_2 are fitting parameters determined from absolute calibration [Nath *et al*, 1993]. For this experiment C_1 equals -28.5 and C_2 equals 0.685, calibrated by Apfel Enterprises Inc.

The experiment consisted of 5 SDDs being employed with each of the 18 MV and 15 MV beams. It was decided that the vials should be used outside the primary beam in case photoneutron production due to high energy x-rays within the detectors was a problem as has been reported by Nath *et al.*, [1993]. The set-up included a slab of styrofoam into which the vials were placed at distances of 10, 15, 20, 30, and 50 cm from the isocentre in the patient plane (see figure 4.2). The field sizes were varied from 10x10 to 30x30 cm^2 for the 18 MV beam, and only 10x10 field size was used for the 15 MV beam. 300 monitor units (MU) was the dose given to the detectors at a dose rate of 300

[+] Apfel Enterprises Inc., New Haven, CT.

MU per minute.

The SDD results must be corrected for temperature because they are sensitive to fluctuations. This is a potential disadvantage for field use because thermal stability needs to be achieved. The results must also be corrected for field size.

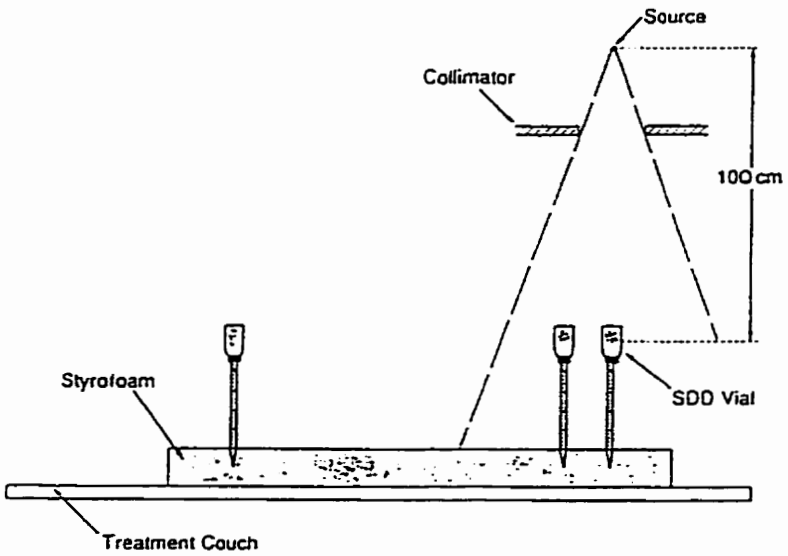

Figure 4.2 Experimental set-up

Nath *et al.*, [1993] found the SDDs to be insensitive to photons with energies below about 6 MV. The detectors were irradiated with 4 MV x-rays. Photon doses of several thousands of centigrays were needed to nucleate any bubbles at all.

4.3 Results & Discussion

The systematic error for the volume displacement readings of these detectors was taken to be +/- 0.005 ml. The vials could only be read to 0.2 ml, out of a possible 6 ml, before they were considered to have absorbed too much dose and thus were insensitive to

further radiations. The results were corrected for temperature but due to the small error in temperature readings, this only led to an error of 0.05% of the volume data. Thus the error in the temperature readings was considered to be neglible and was ignored.

Only two trials for the 15 MV, 10 x 10 cm^2 were acceptable to use for data analysis. Figure 4.3 shows the results for this experiment. One can note that outside the beam with respect to distance from the isocenter the reading seems to be stable around 0.15 to 0.20 mSv / photon Gy. As foreseen this data implies a constant flux of thermal neutrons due to room scattering.

The second set of vials used outside the 18 MV beam have their results depicted in Figure 4.4. As expected the dose equivalence at the 10 cm position increases with field size (ie; as the field begins to encompass that detector). This is due to the increased number of neutrons within the field because they have not been scattered away. Outside the primary beam, the dose equivalence seems to be constant at approximately 0.3 mSv / photon Gy, with respect to distance from the isocentre.

Figure 4.5 is a graphical comparison of the results from both experiments. One can see that the data for the 18 MV beam is roughly a factor of two and a half greater than that from the 15 MV experiment. This results from the increased production of neutrons at higher x-ray energies.

These detectors are meant to be used only once, and thus to have many trials for statistically reliable data the cost becomes a factor. As well there is a chance of receiving a defective detector, one that would give misleading results (low where they should be high and vice versa). This implies that it would be necessary to use 2 or even 3 detectors

for each site reading to receive a truly reliable and accurate reading. Besides these faults the SDDs seem to have much potential for use in radiation protection, but this data must be compared with proven neutron detection techniques.

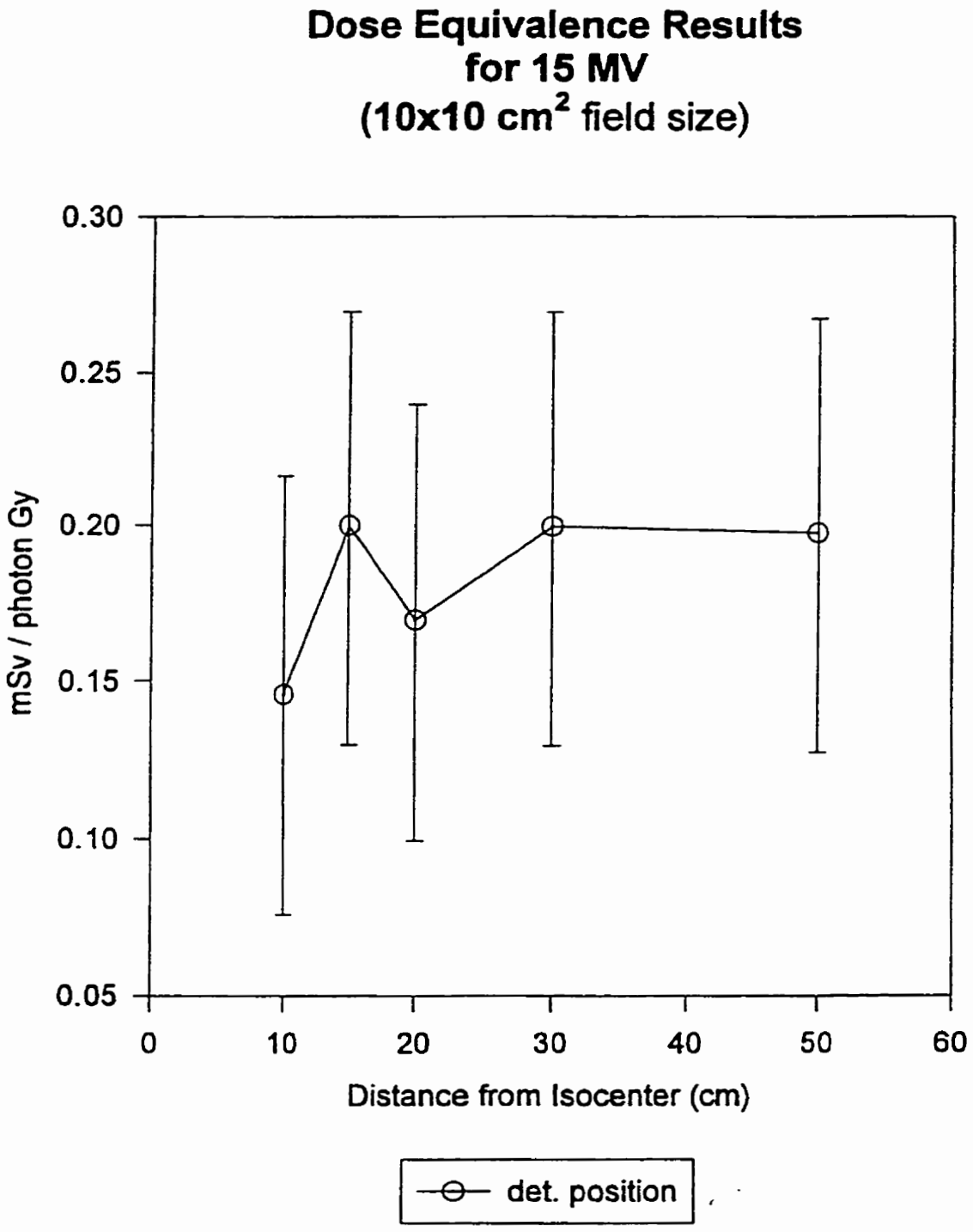

Fig. 4.3 Dose Equivalence Results for 15 MV X-ray beam with a 10x10 cm^2 field size.

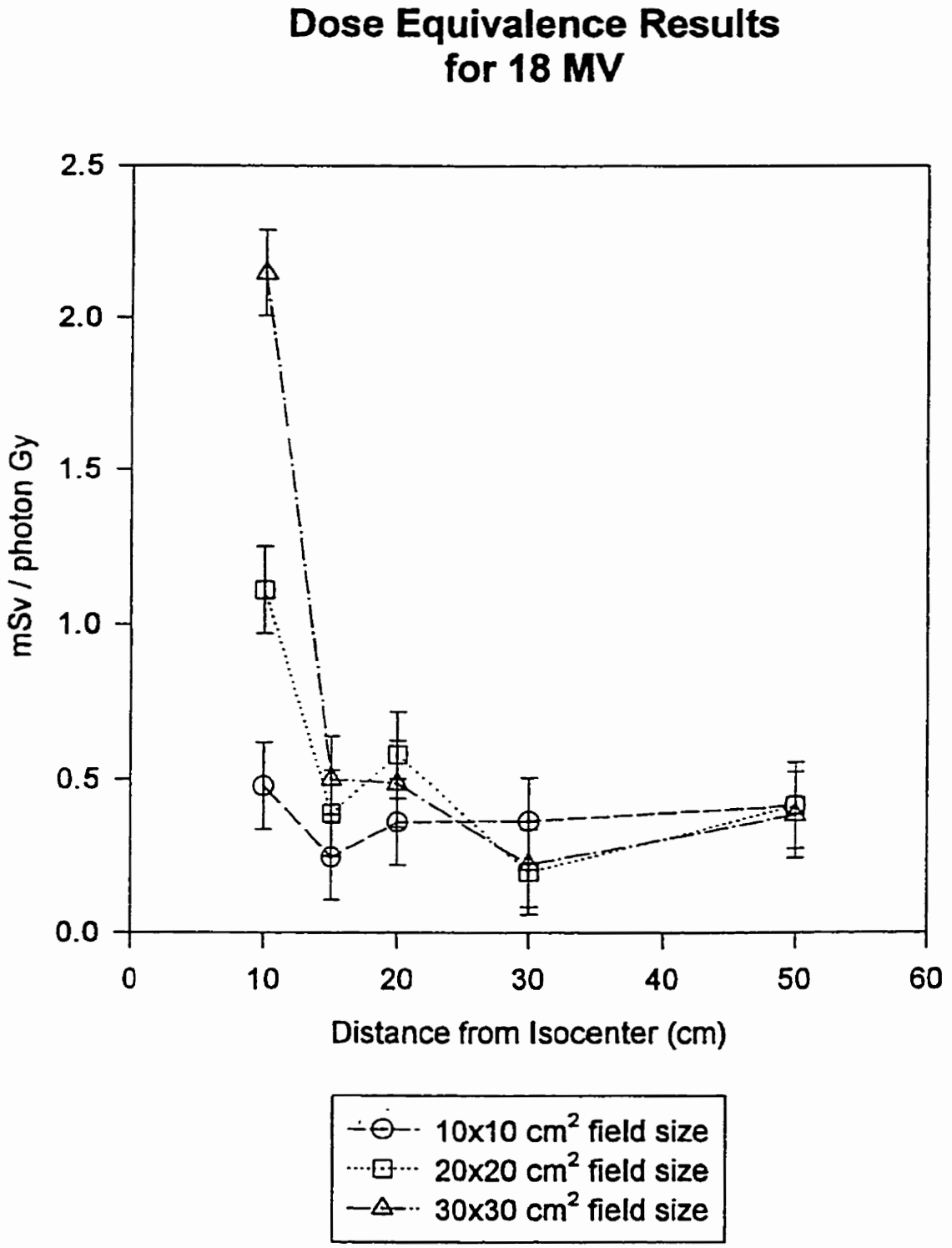

Fig. 4.4 Dose Equivalence Results for 18 MV X-ray beam with field sizes from 10x10 cm^2 to 30x30 cm^2.

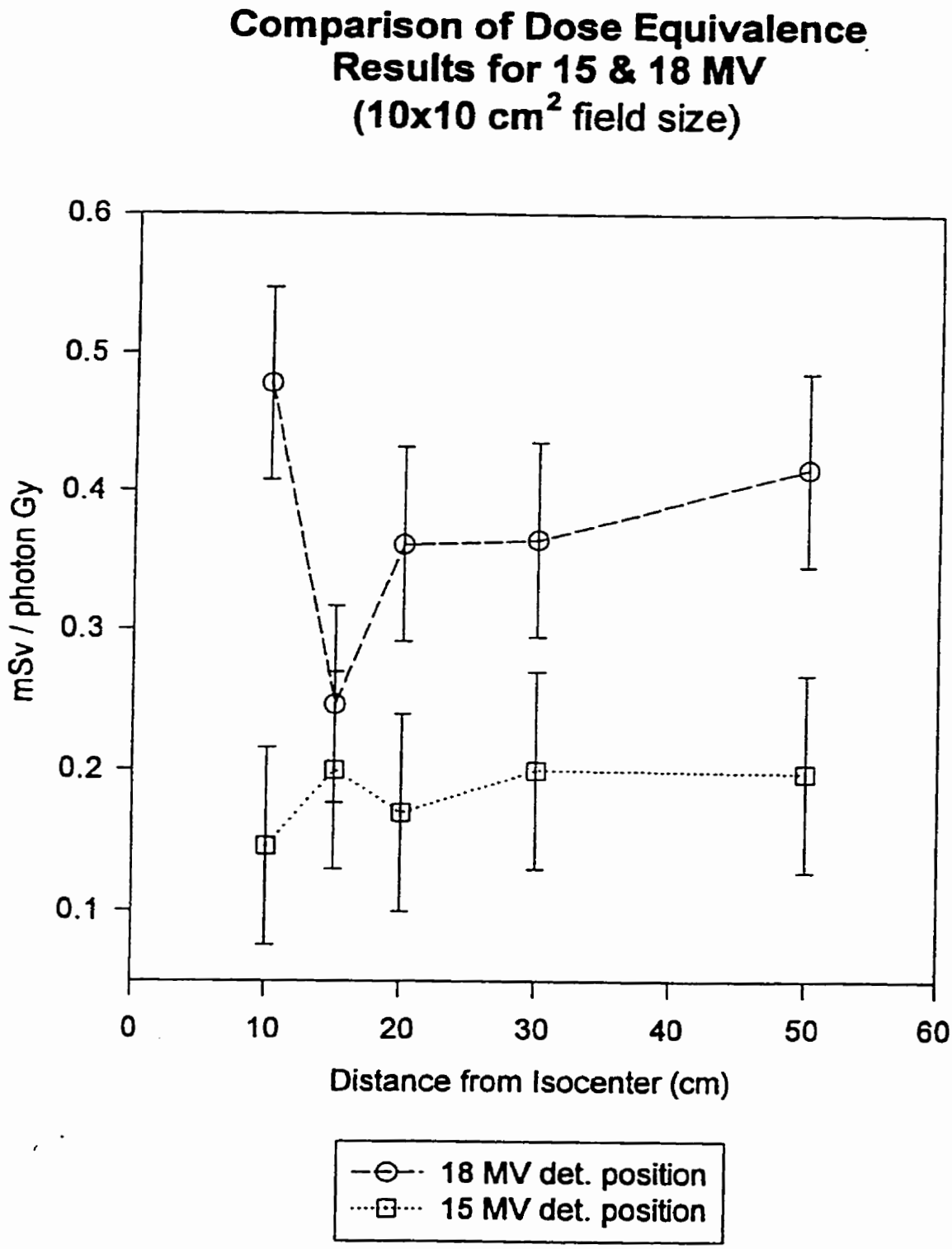

Fig. 4.5 Comparison of Dose Equivalence Results for the 15 and 18 MV X-ray beams with a 10x10 cm^2 field size.

Chapter 5

Comparison and Conclusions

The properties of three neutron detectors have been investigated. Associated with each are advantages and disadvantages. An evaluation of the three detectors can be performed by comparing strong and weak points resulting from the detector designs as well as the data collected in this series of experiments.

Ideally a detector would have the following qualities:

a. low cost

b. not labour intensive

c. a physically small size

d. able to detect a range of neutron energies

e. minimal calculations needed to extract data

f. minimal amount of equipment needed

g. quick reading of results

h. accurate

i. reusable

A detector with all of these characteristics is not currently available. However these qualifications can be used to evaluate the three neutron detectors.

The difficulty with neutron detection is the lack of information about the neutron energy spectrum emanating from the medical electron accelerator. This means that interpretation of measurements in terms of dose equivalence is almost impossible. The

primary photoneutron spectrum may be known but the effects of the photon shielding and the concrete walls enclosing the area have an undetermined and complicated effect on the spectrum. Thus neutron measurements often suffer from one or more problems [McCall *et al*, 1979]. These problems stem from either the detector's response to high energy photons (meaning photoneutron production is occurring within the detector itself and therefore is overestimating the neutron measurements), or the experimenter has made incorrect assumptions concerning the neutron spectrum (whether the detector is measuring fluence or dose equivalence).

In order to evaluate the detectors we compared the individual characteristics to our list of ideal characteristics. These good qualities are then weighed against the shortcomings. As well, a comparison of the data collected from the SDD against the tried and true results from the P_2O_5 and the remmeter will indicate the accuracy and the clinical potential of this new detector.

5.1 Detector #1

Phosphorus pentoxide powder is an activation material which is able to detect a wide range of energies. It is a two part detector, meaning that since it is an activation material it requires the use of a second detector to extract the data gathered by powder. The main problem with P_2O_5 is the preparation of this highly reactive powder. It liquifies when in contact with any moisture (even that in air). One way to get around this problem would be to use orthophosphoric acid whose concentration is known. The second

preparation problem with P_2O_5 deals with the mixture of the P_2O_5 solution (distilled water and powder) with the Liquid Scintillation Counter (LSC) cocktail. Temperatures and concentrations must be experimented with in a trial and error fashion in order to determine an appropriate combination.

A second area of concern is the calculation steps. P_2O_5 powder measures neutron fluence. In order to find the dose equivalence of an exposure, a neutron energy spectrum must be assumed, appropriate conversion factors must also be calculated and utilized. Errors are introduced into this technique as the neutron spectrum becomes moderated. Thus the spectrum changes rapidly as one moves away from the primary photon beam, which necessitates the use of different conversion factors in the phosphorus method. These calculations can introduce a large error into the experiment. The powder also suffers from a lack of sensitivity outside the primary beam.

An advantage is that the P_2O_5 solution (or powder) can be placed in small containers so more than one detector may be used at a time. Also, it should be possible to detect both fast and thermal neutrons simultaneously.

The P_2O_5 dose equivalence results were within experimental error of the calculated Monte Carlo computer simulation results [Liu *et al.*, 1997; Mao *et al.*, 1997; Kase *et al.*, 1997] for the 18 MV beam and were within a factor of two for the 15 MV beam. This detector found less than 0.4% dose within the primary 18 MV beam to be from neutrons and less than 0.07% for the 15 MV beam.

5.2 Detector #2

The remmeter has been around and used for years even though it is known not to be entirely accurate [Rogers, 1979] as it can overestimate the dose equivalence depending on the neutron energies being examined. The activation material within the moderator also requires a second detector to extract the sought after data.

The activation material is a thermal neutron detector which is physically small when used by itself but once the moderator is incorporated into the detector to achieve a remmeter then the whole system becomes rather large (ie; few remmeters may be used at once). The design of the moderator is specific enough that it is difficult to build and is usually commercially bought. If more than one remmeter is to be used at a time this can become expensive. As well, moderators may be designed to allow the measurement of fluence or dose equivalence, independently of neutron energy; in each case, however, the desired aim is only approximated. There is usually a decrease in sensitivity for both low and very high energies. The remmeters are not very sensitive and therefore require long exposure times. The activation remmeter method suffers from significant overresponse in the primary photon beam above 20 MV because of photoneutrons generated in the detector-moderator system [McCall *et al.*, 1984].

The remmeter also needs to be calibrated with a known neutron source. This can become experimentally difficult if a reliable neutron source is not readily available. The use of a second detector and the calculations needed to obtain results delay securing the finished data.

Indium and gold foils are readily available and have a high neutron absorption. Indium is more sensitive due to its shorter half life, but for both materials a decay time is necessary before the foils can be used again. Other advantages are the relative simplicity of its use, and it is insensitive to the specific neutron spectral shape and to the pulsed nature of the radiation.

The foil results were approximately 1000 times too large when Rogers and Dyk's [1981] conversion factor was used. To compensate for this the P_2O_5 results were used as a standard for each field size used in the experiments. The Indium foil results are within experimental error of the P_2O_5 results (or within a factor of two for the 15 MV 20x20 case). The 0x0 field size results are within experimental error of the Monte Carlo computer simulation values. The remmeter found less than 0.32%of the total dose within the 18 MV beam to be from neutrons. Less than 0.18% of the dose was due to neutrons in the 15 MV beam.

5.3 Detector #3

The Superheated Drop Detector is small and very simple to use. Very little amount of calculation is required to determine the dose equivalence. They have not been extensively tested and are reported to be affected by temperature variation. Photoneutron production due to high energy x-rays must also be taken into account when using these detectors. The SDD is not reusable but its low cost offsets this fact. The accuracy of these detectors will be discussed in section 5.4.

This detector determined the percent of the total dose due to neutrons to be less than 0.25% and less than 0.02% for the 18 and 15 MV beams respectively.

5.4 Comparison of Detectors

The remmeter will not be compared with the SDD due to the unusual results obtained by the activation remmeter system. Responses of these neutron detectors depend upon incident neutron energy and the fluence-to-dose conversion factors vary strongly with neutron energy. Great care must be taken when interpreting the readings from neutron remmeters. In the present work, the calibration factor is suspected to be wrong, however, the readings could be expected to be different from predicted results due to photoneutron production occurring in the moderator within the beam, and the change of the neutron quality factor in the late 1980's. The data obtained with the activation remmeter could then still be used to deduce the new dose equivalence but it no longer has its major advantage over most other techniques since one will need to assume a neutron spectral shape [Rogers and Dyk, 1981]. Another possible increase in the dose equivalence found using a remmeter would come from its known overresponse to those neutrons with energies under 100 keV [Rogers, 1979]. Thus it is at best questionable to use remmeters as calibration devices when testing or verifying other types of dosimeters under field conditions [Rogers, 1979]. Usually remmeters provide an adequate radiation protection service in that they err on the conservative side and provide an overestimate of the dose equivalence.

Figures 5.1 to 5.4 are graphical comparisons of the P_2O_5 and the SDD experimental data obtained for this project. In all cases the SDD indicates a smaller dose equivalent reading from just inside the field edge (where the trials start) to approximately 20 cm outside the beam. At this point the SDD and P_2O_5 start to coincide and agree. Since our P_2O_5 results do not show neutrons with energies under the threshold level of 0.7 MeV this might imply that the SDD is detecting a thermal fluence but is not reacting to the higher energy neutrons outside of the photon beam. Our P_2O_5 results decline as the distance from central axis of the primary beam increases. Where the two sets of data seem to coincide (20 cm from the beam edge) could be a result of a decreased amount of high energy neutrons and thus the P_2O_5 results drop off and the SDD is detecting the basic thermalized or scattered component of the neutron spectrum.

Results indicate that the SDD underresponds to the neutron dose equivalence of both the 15 and 18 MV x-ray beams outside of the field. Perhaps if more SDD trials could take place then more information in regards to the statistical error of the SDD results could be found, and hence it might develop that the P_2O_5 and SDD results coincide closer to the beam edge than previously thought.

Near the beam edge the SDD readings are up to 50% less than the P_2O_5 , while further from the field edge the results coincide. Nath *et al.* [1993], found agreement outside the field between P_2O_5 and SDD to ± 5%, however inside the field the SDD™ yielded values 20% higher in a 25 MV x-ray beam from a Sagittaire medical accelerator. Perhaps the SDD is an inefficient neutron detector and it is only because a 25 MV beam was used that they obtained these results. Moderately superheated detectors ($\Delta P < 5$

atm. , ours is approximately 0.81) are sensitive to gamma and x-rays above 6 MeV (it is comparable to the binding energy per nucleon). Thus the probability of photonuclear interactions increase with increasing x-ray energy and heavy ions with sufficient energy to create a bubble are produced. These interactions could be responsible for the high readings in Nath *et al.*'s work. Figure 5.5 shows their work and compares P_2O_5 and the SDD. In figure 5.5 just outside the beam edge the difference in readings is approximately 50% that the SDD underresponds compared with the P_2O_5 results. Further away from the beam edge the results are within the ± 5% agreement. In figure 5.4 one can see the 18 MV comparison of the two detectors for the 30x30 field size. The dose equivalence found inside the beam, at 10 cm from the isocenter, show the SDD to be still underresponding compared to the P_2O_5 results whereas in the Nath *et al.* [1993] report of the 25 MV comparison the SDD results are 20% greater. This data implies that the SDD will overrespond compared to the P_2O_5 technique when a high energy neutron component is present in the beam. As the primary x-ray beam energy increases so does the probability of photonuclear interactions which is most likely the cause of Nath *et al.*'s increased SDD dose equivalence within the primary beam.

In figures 5.6 and 5.7 scatter diagrams of the SDD results versus the P_2O_5 results are shown. The correlation coefficients for the data are 0.94 and 0.83 for the 20x20 cm field size (fig. 5.6) and 30x30 cm field size (fig. 5.7) respectively. A linear regression was performed for both scatter diagrams and the equations of these lines are,

$$Y(SDD) = 0.51 * X(P_2O_5) - 0.11 \qquad (r = 0.94)$$

$$Y(SDD) = 0.66 * X(P_2O_5) - 0.48 \qquad (r = 0.83)$$

The SDD is versatile, small in size and extremely simple to use. However it seems the accuracy of the SDD is questionable in and close to the primary x-ray beam. Nath *et al.* [1993] reports the accuracy of the SDD as ± 20% and that this is quite acceptable for measurement of a contaminant field. It has been shown that the accuracy of the SDD is not ± 20% but ± 50%, and the instrument is underresponding compared to the P_2O_5 results. Thus it does not err on the conservative side as the work done by Nath *et al.* [1993] would seem to indicate. This leads one to the conclusion that the SDD are useful and accurate only when detecting the thermalized or scattered component of the neutron spectrum from a medical electron accelerator.

Four main conclusions can be drawn from the results of this project. These are:

1. The SDD underresponds compared to the P_2O_5.

2. The remmeter needs a known neutron source to calculate a conversion factor for saturation activity to dose equivalent. Otherwise it requires a standard (used from experimental or computational results) for each field size in question.

3. The P_2O_5 detector is reliable and effective if a proper neutron energy spectrum estimation is used.

4. According to the P_2O_5 results < 0.40% and < 0.07% of the total dose is due to neutrons for the 18 and 15 MV beams respectively of a Varian linac.

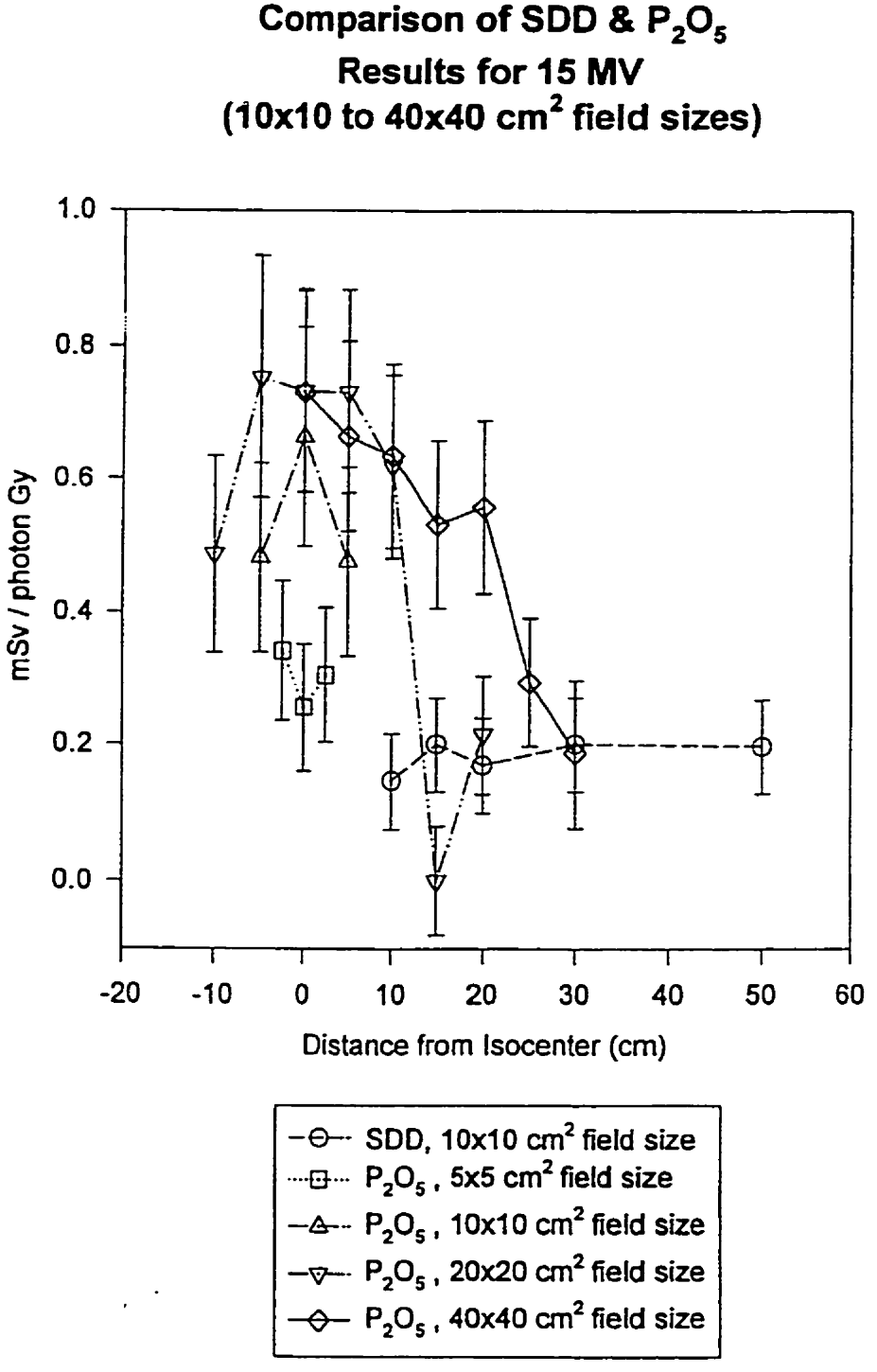

Fig. 5.1 Comparison of SDD and P_2O_5 Dose Equivalence Results for the 15 MV X-ray beam. Field sizes ranging from 10x10 cm^2 to 40x40 cm^2 for P_2O_5, and 10x10 cm^2 for the SDD.

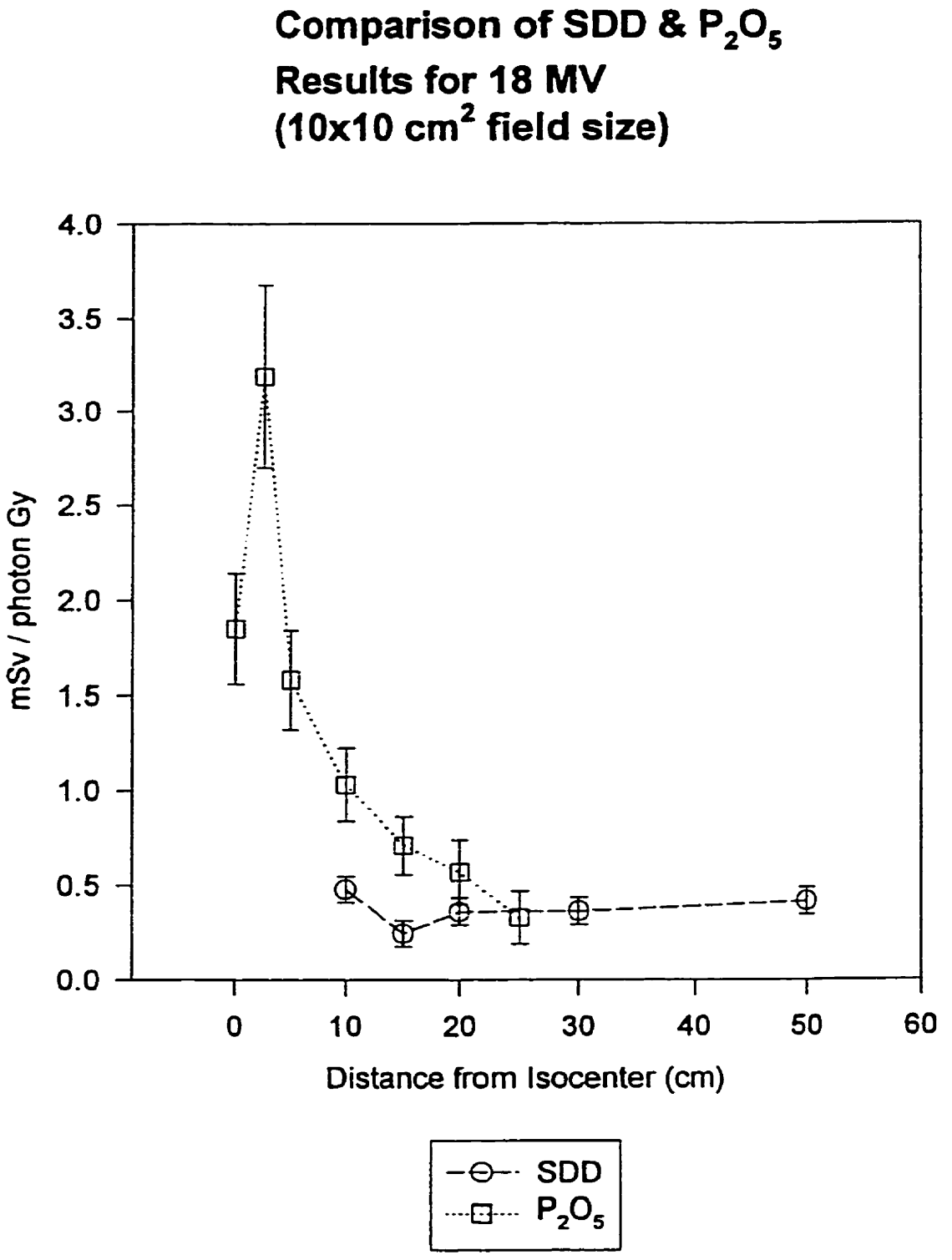

Fig. 5.2 Comparison of SDD and P_2O_5 Dose Equivalence Results for the 18 MV X-ray beam with a 10x10 cm^2 field size.

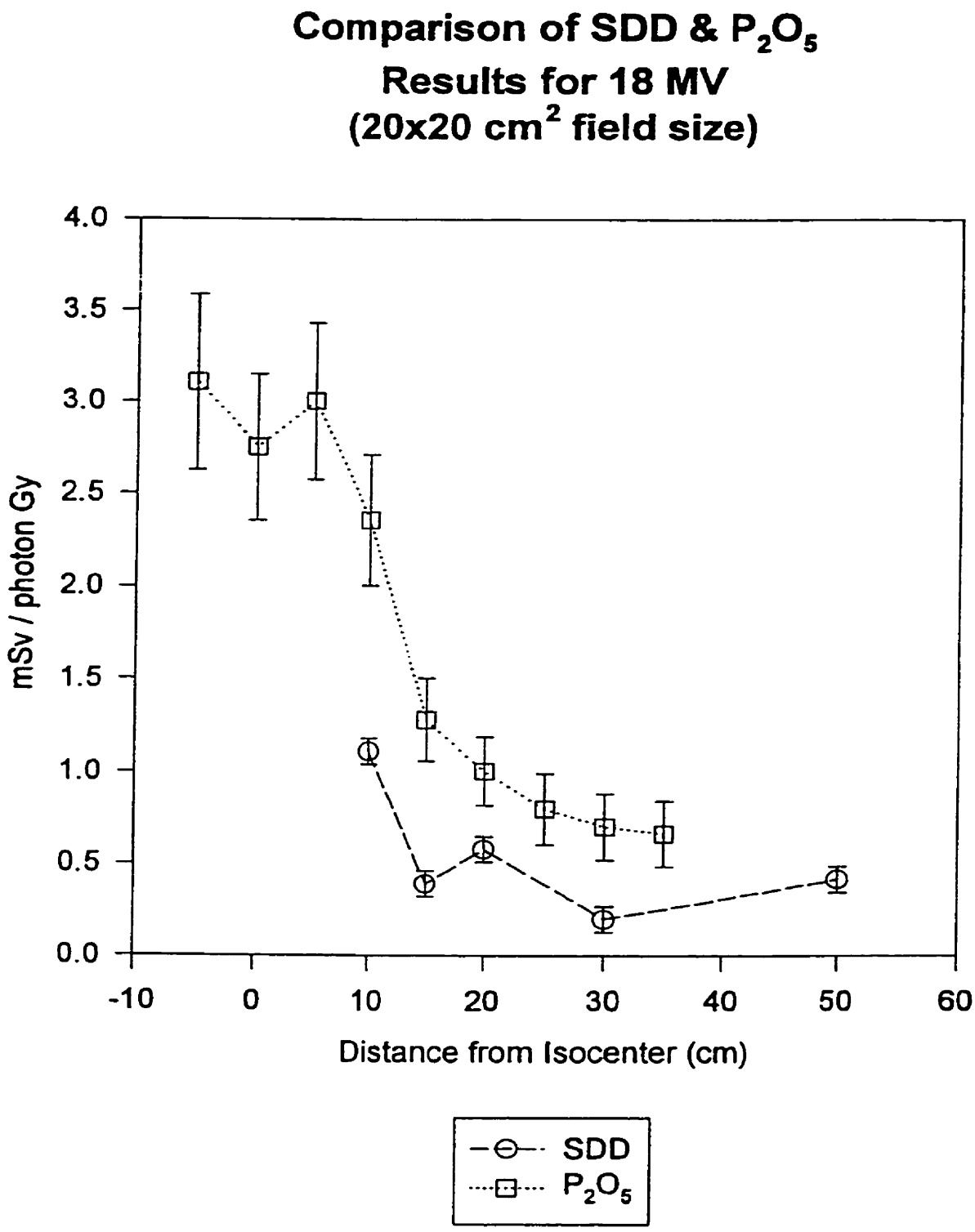

Fig. 5.3 Comparison of SDD and P_2O_5 Dose Equivalence Results for the 18 MV X-ray beam with a 20x20 cm^2 field size.

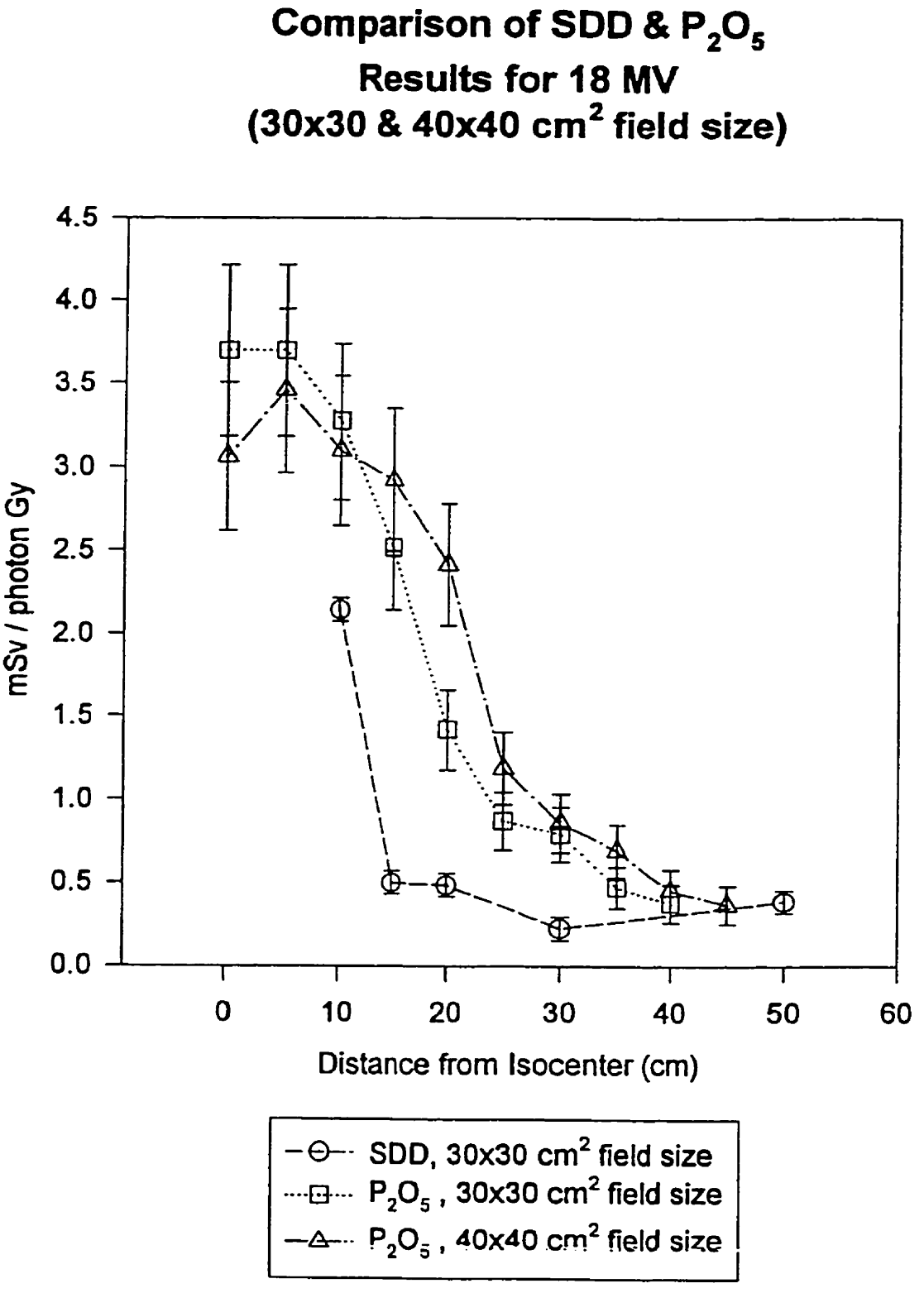

Fig. 5.4 Comparison of SDD and P_2O_5 Dose Equivalence Results (18 MV X-ray beam, a 30x30 cm^2 field size for the SDD and both 30x30 and 40x40 cm^2 field sizes for the P_2O_5).

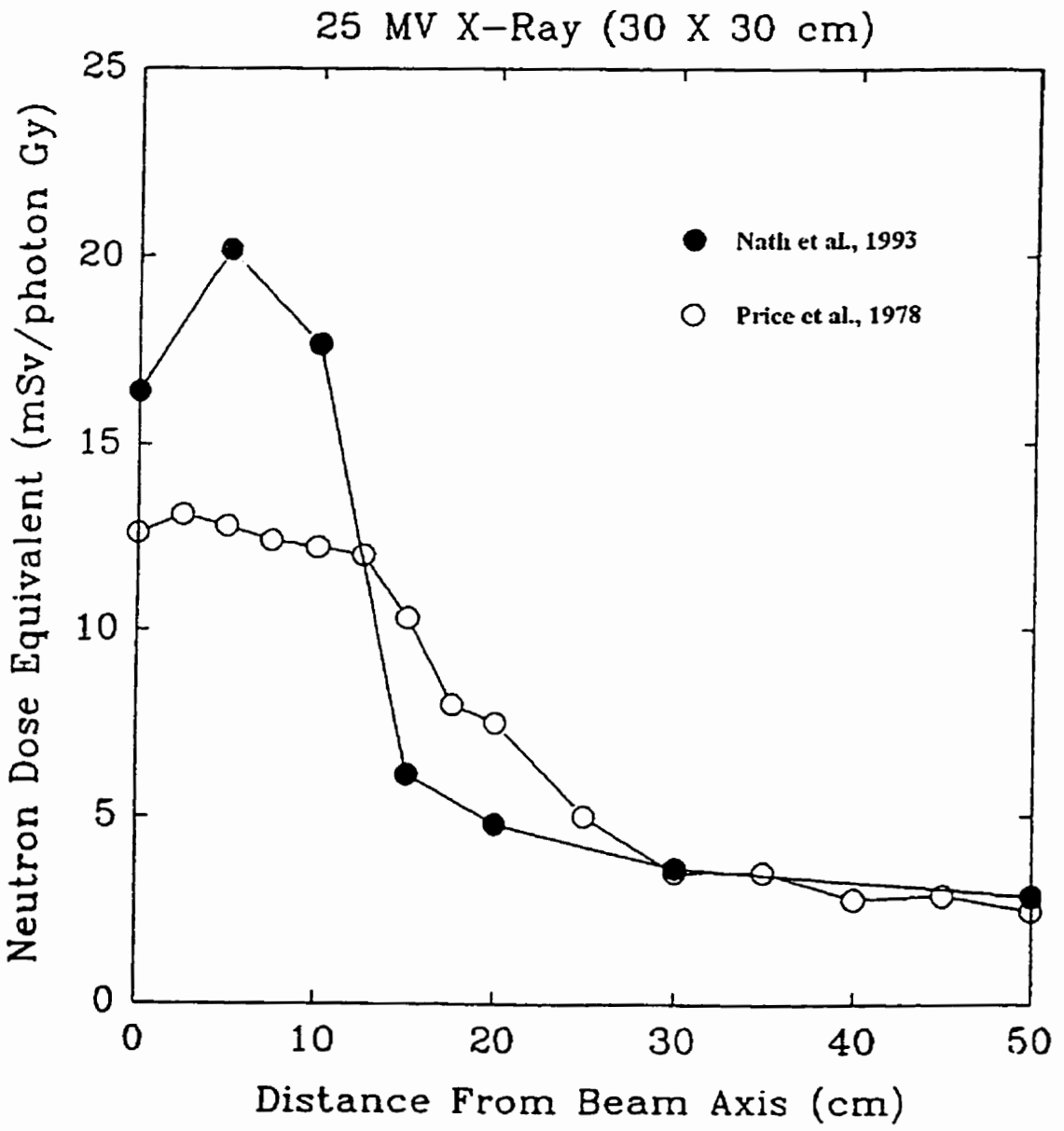

Fig. 5.5 Comparison of work done by Nath *et al.* [1993] using the SDD and Price *et al.* [1978] using P_2O_5.

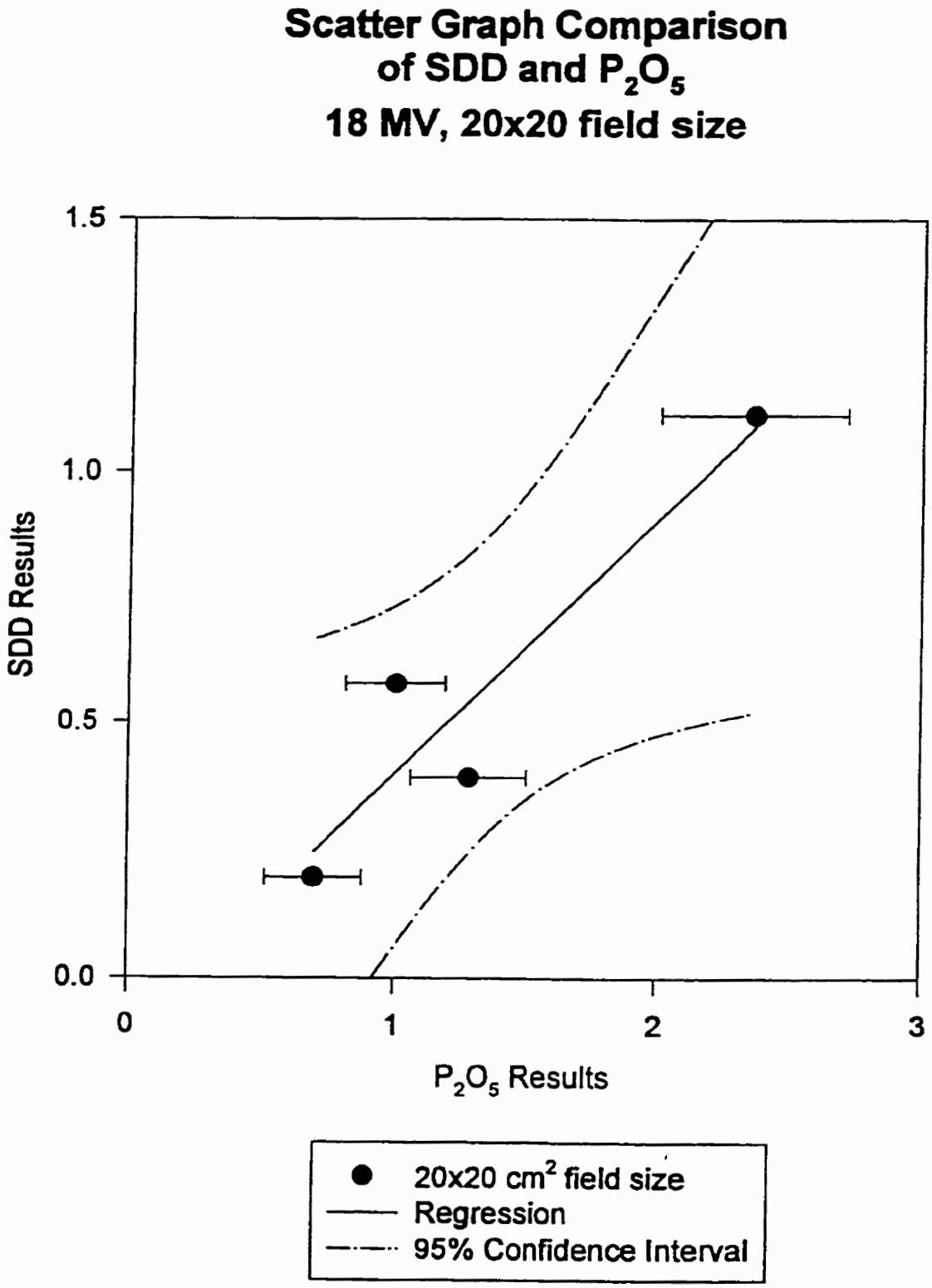

Fig. 5.6 Scatter Diagram of SDD Results verses P_2O_5 Results for the 18 MV X-ray beam with a 20x20 cm^2 field size. A Linear Regression was done with a 95% Confidence Interval.

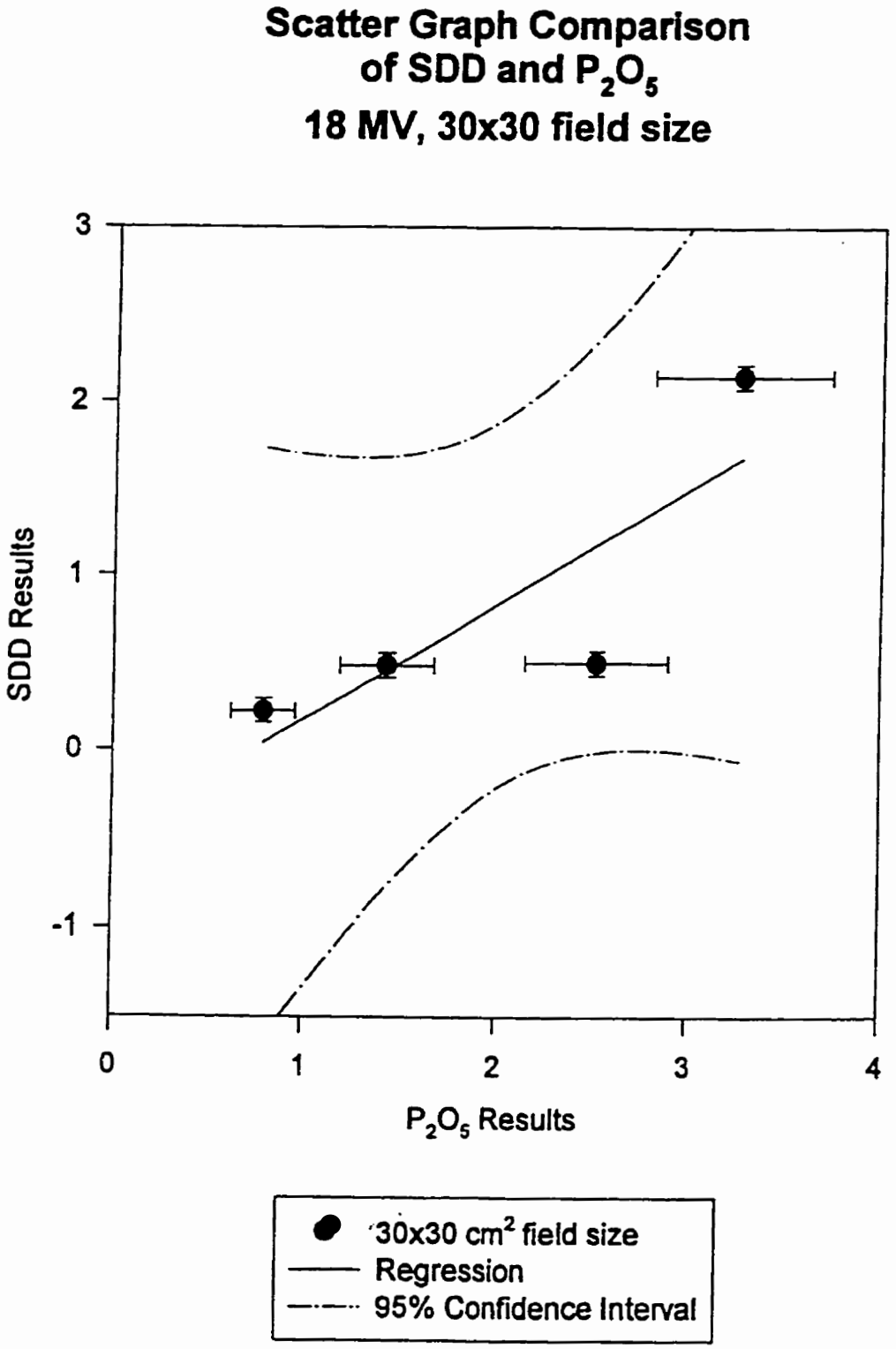

Fig. 5.7 Scatter Diagram of SDD Results verses P_2O_5 Results for the 18 MV X-ray beam with a 30x30 cm^2 field size. A Linear Regression was done with a 95% Confidence Interval.

Bibliography

Agosteo, S., Foglio Para, A., Maggioni, B., Sanguist, V., Terrani, S., & Borasi, G. (1995). Radiation Transport in a Radiotherapy Room. Health Physics, 68, 1, 27-34.

Allen, P.D., & Chaudhri, M.A. (1988). Photoneutron production in tissue during high energy bremsstrahlung radiotherapy. Physics in Medicine and Biology, 33, 9, 1017-1036.

Allen, P.D., & Chaudhri, M.A. (1991). Production of neutrons from water, polyethylene, tissue equivalent material and CR-39 irradiated with 2.5-30 MeV photons. Australasian Physical and Engineering Sciences in Medicine, 14, 3, 153-156.

Apfel, R.E. (1979). The superheated drop detector. Nuclear Instruments and Methods, 162, 603-608.

Apfel, R.E., & Lo, Y.-C. (1989). Practical neutron dosimetry with superheated drops. Health Physics, 56, 79-83.

Apfel, R.E., & Roy, S.C. (1984). Investigations on the applicability of superheated drop detectors in neutron dosimetry. Nuclear Instruments and Methods in Physics Research, 219, 582-587.

Bading, J.R., Zeitz, L., & Laughlin, J. (1982). Phosphorus activation neutron dosimetry and its application to an 18-MV radiotherapy accelerator. Medical Physics, 9, 6, 835-843.

Batenkov, O.I. (1983). "Experimental and theoretical investigation of the energy distribution of Californium-252 spontaneous fission neutrons". International Nuclear Data Committee, IAEA Nuclear Data Section, Vienna.

Garber, D.I., & Kinsey, R.R. (1976). "Neutron Cross Sections, Volume II, Curves". Information Analysis Center Report, BNL 325, Brookhaven National Laboratory.

Grimeland, E., Jellsby, K., & Vines, J. (1964). Cross sections of some reactions induced in nitrogen, phosphorus, copper, and bromine with neutrons of energy 14.8 MeV. Physical Review, 137, 4b, b878-b882.

Grundl, J.A., Henuel, R.L., & Perkins, B.L. (1958). $^{31}P(n,p)^{31}Si$ and $^{27}Al(n,\alpha)^{24}Na$ Cross Sections. Physical Review, 109, 2, 425-428.

Gur, D., Rosen, J.C., Bukovitz, A.G., & Gill, A.W. (1978). Fast and slow neutrons in an 18-MV photon beam from a Phillips SL/75-20 linear accelerator. Medical Physics, 5, 3, 221-222.

Hall, E.J. (1988). "Radiobiology for the Radiologist", 3rd Ed. J.B. Lippincott Company, Philadelphia, U.S.A.

Henderson, C. (1970). "Cloud and Bubble Chambers". Butler & Tanner Ltd, London, Great Britain.

Hughes, D.J. (1957). "Neutron Cross Sections". Pergamon Press, Brookhaven National Laboratory.

IAEA Technical Report Series 107 (1970). " Neutron Fluence Measurements". IAEA Publications, Vienna.

IAEA Technical Report Series 156 (1974). "Handbook on Nuclear Activation Cross-Sections". IAEA Publications, Vienna.

IAEA Technical Report Series 252 (1985). "Neutron Monitoring for Radiological Protection" IAEA Publications, Vienna.

ICRP Publications 15 and 21 (1978). "Protection against Ionizing Radiation from External Sources" and "Data for Protection against Ionizing Radiation from External Sources". Pergamon Press, Toronto, Ontario, Canada.

ICRP Publication 51 (1987). "Data for Use in Protection Against External Radiation". Pergamon Press, Toronto, Ontario, Canada.

ICRP Publication 60 (1990). "1990 Recommendations of the International Commission on Radiological Protection". Pergamon Press, Toronto, Ontario, Canada.

ICRU Report 33 (1980). "Radiation Quantities and Units". ICRU Publications, Washington, D.C., U.S.A.

ICRU Report 36 (1983). "Microdosimetry". ICRU Publications, Bethesda, Maryland, U.S.A.

Ing, H., Nelson, W.R., & Shore, R.A. (1982). Unwanted photon and neutron radiation resulting from collimated photon beams interacting with the body of radiotherapy patients. Medical Physics, 9, 1, 27-33.

Ing, H., & Shore, R.A. (1982). Unwanted radiation produced by leakage neutrons from medical electron accelerators. Medical Physics, 9, 1, 34-36.

Jackson, J.D. (1975). "Classical Electrodynamics", 2nd Ed. John Wiley & Sons, Toronto, Canada.

Johns, H.E., & Cunningham, J.R. (1983). "The Physics of Radiology", 4th Ed. Charles C. Thomas - Publisher, Springfield, Illinois, U.S.A.

Kase, K.R., Mao, X.S., Nelson, W.R., Liu, J.C., Kleck, J.H., & Elsalim, M. (1997). Neutron fluence and Energy Spectra Around the Varian Clinac 2100C/2300C Medical Accelerator. Health Physics, (revised manuscript returned to journal).

Karzmark, C.J., Nunan, C.S., & Tanabe, E. (1993). "Medical Electron Accelerators". McGraw-Hill, Inc., Health Professions Division, Toronto, Canada.
Knoll, G.F. (1989). "Radiation Detection and Measurement", 2nd Ed. John Wiley & Sons, Inc., Toronto, Canada.

Krane, K.S. (1988). "Introductory Nuclear Physics". John Wiley & Sons, Inc., Toronto, Canada.

Levinger, J.S., & Bethe, H.A. (1950). Dipole transitions in the nuclear photo-effect. Physical Review, 78, 2, 115-129.

Liu, J.C. (1995). TLD/ Bonner Sphere Spectrometer Data - Private Communication.

Liu, J.C., Kase, K.R., Mao, X.S., Nelson, W.R., Kleck, J.H., & Johnson, S. (1997). Calculations of Photoneutrons from Varian Clinac Accelerators and Their Transmissions in Materials. SLAC-PUB-7404.

Liu, J.C., Nelson, W.R., Kase, K.R., & Mao, X.S. (1997). Calculations of the giant-dipole-resonance photoneutrons using a coupled EGS4-MORSE code. Radiation Protection Dosimetry, 70, 1-4, 49-54.

Mao, X.S., Kase, K.R., Liu, J.C., & Nelson, W.R. (1996). Giant dipole resonance neutron yields produced by electrons as a function of target material and thickness. Health Physics, 70, 2, 207-214.

Mao, X.S., Kase, K.R., Liu, J.C., Nelson, W.R., Kleck, J.H., & Johnson, S. (1997). Neutron sources in the Varian Clinac 2100C/2300C medical accelerator calculated by the EGS4 code. Health Physics, 72, 4, 524-529.

McCall, R.C., Almond, P.R., Holeman, G.R., Devanney, J.A., Lanzl, L.H., & Fuller, E.G. (1984). "Neutron Contamination from medical electron accelerators". NCRP Report 79. Bethesda, Maryland, U.S.A.

McCall, R.C., Jenkins, T.M., & Shore, R.A. (1979). Transport of accelerator produced neutrons in a concrete room. IEEE Transactions on Nuclear Science, NS-26, 1, 1593-1597.

McCall, R.C., Jenkins, T.M., & Tochilin, E. (1976). "High energy photon response of moderated neutron detectors". Stanford Linear Accelerator Center Publication - 1768.

McGinley, P.H., Wood, M., Mills, M., & Rodriguez, R. (1976). Dose levels due to neutrons in the vicinity of high-energy medical accelerators. Medical Physics, 3, 6, 397-402.

Nath, R., Boyer, A.L., La Riviere, P.D., McCall, R.C., & Price, K.W. (1986). "Neutron Measurements around high energy x-ray radiotherapy machines". AAPM Report 19. American Institute of Physics, Inc. New York, New York, U.S.A.

Nath, R., Epp, E.R., Laughlin, J.S., Swanson, W.P., & Bond, V.P. (1984). Neutrons from high-energy x-ray medical accelerators: An estimate of risk to the radiotherapy patient. Medical Physics, 11, 3, 231-241.

Nath, R., Meigooni, A.S., King, C.R., Smolen, S., & d'Errico, F. (1993). Superheated drop detector for determination of neutron dose equivalent to patients undergoing high-energy x-ray and electron radiotherapy. Medical Physics, 20, 3, 781-787.

Nath, R., Price, K.W., & Holeman, G.R. (1980). An intercomparison of neutron measurements for a 25 MV x-ray radiotherapy accelerator. Medical Physics, 7, 5, 545-548.

Palta, J.R., Hogstrom, K.R., & Tannanonta, C. (1984). Neutron leakage measurements from a medical linear accelerator. Medical Physics, 11, 4, 498-501.

Price, K.W., Holeman, G.R., & Nath, R. (1978). A technique for determining fast and thermal neutron flux densities in intense high-energy (8-30 MeV) photon fields. Health Physics, 35, 341-351.

Price, K.W., Nath, R., & Holeman, G.R. (1978). Fast and thermal neutron profiles for a 25-MV x-ray beam. Medical Physics, 5, 4, 285-289.

Riel, G., Rao, N., Kerschner, H., & Nelson, M. (1991). Superheated drop, 'Bubble', neutron dosimeter performance in a work enviroment. IEEE Transactions on Nuclear Science, 38, 2, 494-496.

Rogers, D.W.O. (1979). Why not to trust a neutron remmeter. Health Physics, 37, 735-742.

Rogers, D.W.O., & Dyk, G.V. (1981). Use of a neutron remmeter to measure leakage neutrons from medical electron accelerators. Medical Physics, 8, 2, 163-166.

Roy, S.C., Apfel, R.E., & Lo, Y.-C. (1987). Superheated drop detector: A potential tool in neutron research. Nuclear Instruments and Methods in Physics Research, A255, 199-206.

Sanchez, F., Madurga, G., & Arrans, R. (1989). Neutron measurements around an 18 MV linac. Radiotherapy and Oncology, 15, 259-265.

Sorenson, J.A., & Phelps, M.E. (1987). "Physics in Nuclear Medicine", 2nd Edition. W.B. Saunders Company, Toronto.

Stranden, E. (1977). Activity induced in patients by high energy x-ray therapy. Physics in Medicine and Biology, 22, 2, 348-352.

Stephens, L.D., & Smith, A.R. (1958). Fast-neutron surveys using indium-foil activation. UCRL-8418. Berkeley, California, U.S.A.

Swanson, W.P. (1978). Calculation of neutron yields released by electrons incident on selected materials. Health Physics, 35, 353-367.

Swanson, W.P. (1979). Improved calculation of photoneutron yields released by incident electrons. Health Physics, 37, 347-358.

Swanson, W.P. (1980). Estimate of the risk in radiation therapy due to unwanted neutrons. Medical Physics, 7, 2, 141-144.

Tosi, G., Torresin, A., Agosteo, S., Foglio Para, A., Sanguist, V., Zeni, L., & Silari, M. (1991). Neutron measurements around medical electron accelerators by active and passive detection techniques. Medical Physics, 18, 1, 54-60.

Uwamino, Y., Nakamura, T., & Ohkubo, T. (1986). Measurement and calculation of neutron leakage from a medical electron accelerator. Medical Physics, 13, 3, 374-384.

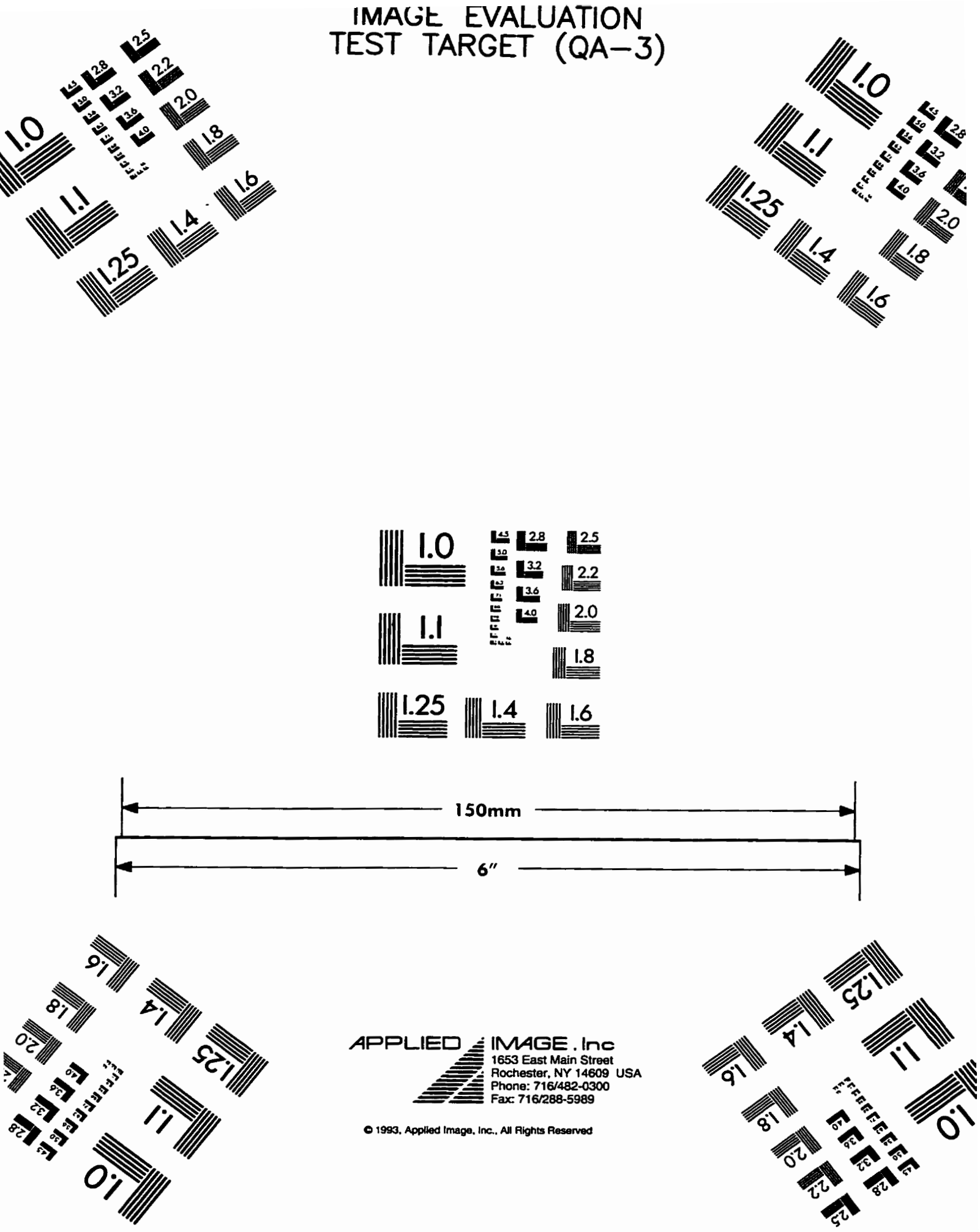
IMAGE EVALUATION
TEST TARGET (QA-3)
1.0
1.1
1.25
1.4
1.6
1.8
2.0
2.2
2.5
2.8
3.2
3.6
4.0
150mm
6"
APPLIED IMAGE, Inc
1653 East Main Street
Rochester, NY 14609 USA
Phone: 716/482-0300
Fax: 716/288-5989
© 1993, Applied Image, Inc., All Rights Reserved